AGU PUBLICATIONS

JGR

Journal of Geophysical Research: Planets

RESEARCH ARTICLE
10.1002/2016JE004998

Key Points:
- The ratio of intrusive to extrusive magmatism is higher at Syrtis Major and Tharsis than on Earth
- We consider possible controls on the intrusion versus eruption of Martian magmas
- Crustal heating, weak time-averaged recharge, and volatile-poor magmas favored intrusive magmatism at Syrtis Major and Tharsis

Correspondence to:
B. A. Black,
bblack@ccny.cuny.edu

Citation:
Black, B. A., and M. Manga (2016), The eruptibility of magmas at Tharsis and Syrtis Major on Mars, *J. Geophys. Res. Planets*, *121*, doi:10.1002/2016JE004998.

Received 18 NOV 2015
Accepted 13 APR 2016
Accepted article online 28 APR 2016

The eruptibility of magmas at Tharsis and Syrtis Major on Mars

Benjamin A. Black[1,2] and Michael Manga[2]

[1]Department of Earth and Atmospheric Science, City College, City University of New York, New York City, New York, USA, [2]Department of Earth and Planetary Science, University of California, Berkeley, California, USA

Abstract Magnetic and geologic data indicate that the ratio of intrusive to extrusive magmatism (the *I/E* ratio) is higher in the Tharsis and Syrtis Major volcanic provinces on Mars relative to most volcanic centers on Earth. The fraction of magmas that erupt helps to determine the effects of magmatism on crustal structure and the flux of magmatic gases to the atmosphere and also influences estimates of melt production inferred from the history of surface volcanism. We consider several possible controls on the prevalence of intrusive magmatism at Tharsis and Syrtis Major, including melt production rates, lithospheric properties, regional stresses and strain rates, and magmatic volatile budgets. The Curie temperature is the minimum crustal temperature required for thermal demagnetization, implying that if the primary magnetic mineral is magnetite or hematite, the crust was warm during the intrusive magmatism reflected in Tharsis and Syrtis Major *I/E* ratios. When wall rocks are warm, thermally activated creep relaxes stresses from magma replenishment and regional tectonics, and eruptibility depends on buoyancy overpressure. We develop a new one-dimensional model for the development of buoyancy in a viscous regime that accounts for cooling, crystallization, volatile exsolution, bubble coalescence and rise, fluid egress, and compaction of country rock. Under these conditions, we find that initial water and CO_2 contents typically <1.5 wt % can explain the observed range of intrusive/extrusive ratios. Our results support the hypothesis that warm crust and a relatively sparse volatile budget encouraged the development of large intrusive complexes beneath Tharsis and Syrtis Major.

1. Introduction

On Mars, as on Earth, some magmas freeze in the crust and some magmas erupt. The relative proportion of intrusive versus extrusive magma volumes (the *I/E* ratio) determines the structure and flexural state of the crust and the efficiency and speciation of degassing [e.g., *Greeley and Schneid*, 1991; *Phillips et al*., 2001; *O'Neill et al*., 2007; *Hirschmann and Withers*, 2008; *Jellinek et al*., 2008; *Grott et al*., 2011]. Gas release during magmatism (both intrusive and extrusive) exerts an important control on atmospheric composition and may have contributed to more clement conditions on early Mars [e.g., *O'Neill et al*., 2007; *Halevy and Head*, 2014]. However, both the relative magnitude of intrusive and extrusive magmatism at different locations on Mars and the processes that control the intrusive/extrusive ratio are poorly understood [*Mitchell et al*., 2007; *Lillis et al*., 2008b].

On Earth, volume estimates for intrusive magmatism derive from seismic and gravity data and from mapping of geologic exposures of volcanic-plutonic systems [*White et al*., 2006]. Mapping similarly delimits the volume of volcanic rocks. While the available data do suggest that intrusive/extrusive ratios may tend toward higher values in settings with thickened crust [e.g., *Ward et al*., 2014], in general, intrusive/extrusive ratios on Earth predominantly range in value from 1 to 10, with significant regional dispersal and little systematic correlation with composition or total volume [*Crisp*, 1984; *White et al*., 2006].

On Mars, gravity and magnetic data provide the best constraints on the *I/E* ratio. Orbital magnetic mapping has revealed that large swaths of Mars, in particular in the vicinity of impact basins and magmatic centers, have relatively weak remanent magnetizations [*Acuna et al*., 1999; *Johnson and Phillips*, 2005; *Lillis et al*., 2008b]. This observation is consistent with the existence of an ancient, now-extinct Martian dynamo that generated crustal magnetic remanence, which has subsequently undergone local impact or thermal demagnetization [*Lillis et al*., 2008a; *Roberts et al*., 2009]. In the Tharsis and Syrtis Major volcanic centers, where heating during magmatism is the most likely cause of crustal demagnetization, stochastic models that combine sill and dike emplacement and heat transfer have placed constraints on the volume of intruded magma [*Lillis et al*., 2009, 2015]. Comparison with volume estimates for nearby extrusive rocks indicates that the

Table 1. Estimated Intrusive and Extrusive Magma Volumes on Mars, the Ratio of Intrusive to Extrusive Volumes, and the Range of Terrestrial Intrusive/Extrusive Ratios

Location	Intrusive Volume (km^3)	Extrusive Volume (km^3)	Intrusive/Extrusive Ratio	Method	References
Tharsis (Arsia Mons region; 240°E, 10°S)	$0.6–1.8 \times 10^6$ km^3	$0.0025–0.2 \times 10^6$ km^3	3–750	Magnetic/geologic mapping	*Lillis et al.* [2009] and *Bleacher et al.* [2009]
Tharsis (overall)	$3–10 \times 10^8$ km^3	3.5×10^7 km^3	9–29	Extrapolation of intrusive thicknesses from *Lillis et al.* [2009]	*Head et al.* [2002] and this study
Syrtis Major (67°E, 8°N)	$4–19 \times 10^6$ km^3	$0.16–0.32 \times 10^6$ km^3	12.5–120	Magnetic/geologic mapping	*Hiesinger and Head* [2004] and *Lillis et al.* [2015]
Mars (global)			56–167	^{40}Ar	*Tajika and Sasaki* [1996]
Mars (global)			5–12	Assumed from Earth	*Greeley and Schneid* [1991]
Mars (global)			<100	Volume of the crust relative to total volcanic output (see section 3.4)	*Greeley and Schneid* [1991]
Mars (range)			3–750		
Earth			typically 1–10	See section 2 of the text	*Crisp* [1984] and *White et al.* [2006]

intrusive/extrusive ratio at Tharsis and Syrtis Major appears to be higher than at most localities on Earth (see Table 1), implying that Tharsis and Syrtis Major magmas are less likely to erupt [*Lillis et al.*, 2009, 2015].

To erupt, magmas must be buoyant and overpressures (and the accompanying stresses around the magma chamber) must be sufficient to promote failure of the surrounding rocks and dike propagation toward the surface (Figure 1). The wall rocks are expected to have a Maxwellian viscoelastic rheology, and consequently, the maximum overpressure in the chamber will depend on buoyancy, recharge rates, chamber volume, and the temperature-dependent wall rock viscosity [*Dragoni and Magnanensi*, 1989; *Jellinek and DePaolo*, 2003; *Karlstrom et al.*, 2010; *Karlstrom and Richards*, 2011; *Degruyter and Huber*, 2014; *Caricchi et al.*, 2014]. Surface loading also modulates overpressure [*Pinel and Jaupart*, 2004; *Grosfils*, 2007; *McGovern et al.*, 2013; *de Silva and Gregg*, 2014], and regional stresses and strain rates can influence magma ascent [e.g., *Delaney et al.*, 1986; *Rubin*, 1995; *Buck et al.*, 2006; *Menand et al.*, 2010; *Daniels and Menand*, 2015]. In the limit where viscous relaxation quickly alleviates lithospheric stresses from changes in magma volume or from loading and regional tectonics, buoyancy from volatile exsolution during decompression or second boiling controls eruptibility [*Tait et al.*, 1989; *Caricchi et al.*, 2014; *Malfait et al.*, 2014; *Degruyter and Huber*, 2014].

In this work, we first review the constraints on the *I/E* ratio on Earth and Mars. We then consider several factors that can influence the eruptibility of magmas: rates of melt production, magmatic volatile budgets, lithospheric properties, and regional stresses and strain rates. These factors vary from place to place on

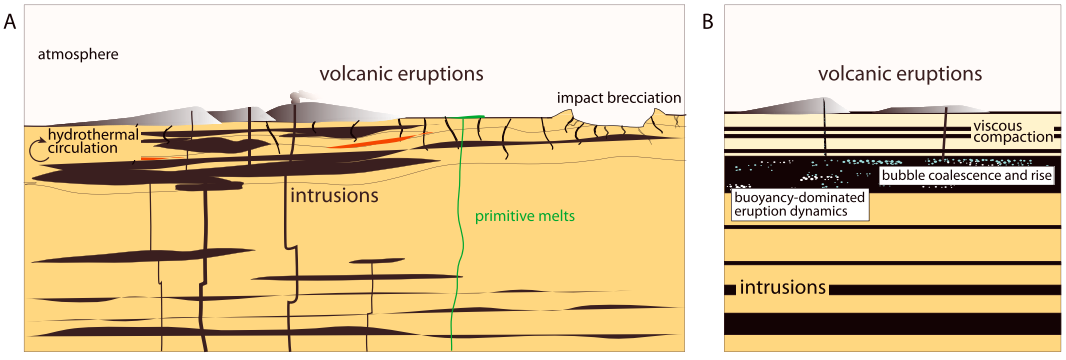

Figure 1. (a) Schematic diagram of a crustal magmatic system on Mars. Impact brecciation may have increased void space in the uppermost several kilometers of the crust [*Clifford*, 1993; *Wilson and Head*, 1994]. Orbital and rover-based spectroscopy provide evidence for some primitive melts (green) that have ascended from the mantle with little crustal interaction [*McSween et al.*, 2006; *Baratoux et al.*, 2011]. (b) Our one-dimensional model focuses on volatile exsolution, bubble coalescence and rise, and the development of buoyancy overpressure in order to determine the conditions under which Martian magmas erupt.

Earth [*Crisp*, 1984] and may also differ considerably between Earth and Mars. These differences arise in large part from contrasting thermal evolution, tectonic regime, and mantle composition on Earth and Mars. In this work, we focus on the implications for conditions in and around magma bodies. We develop a new one-dimensional model for magmatic systems in the viscous regime that tracks the thermochemical evolution of a magma body and the fate of magmatic volatiles. We apply this model in conjunction with published scaling relationships to investigate the causes of elevated *I/E* ratios at Tharsis and Syrtis Major.

2. Intrusive/Extrusive Ratios on Earth

Even on Earth, calculation of *I/E* ratios carries substantial uncertainties [*Crisp*, 1984; *White et al*., 2006]. The major uncertainties in extrusive volumes derive from uncertainties in erosion and present-day thickness [*White et al*., 2006]. Volume snapshots for active magmatic systems can be determined from sulfur degassing [*Allard*, 1997] or seismic, geodetic, or electromagnetic surveys [*White et al*., 2006]. The volumes of exhumed intrusive bodies can be mapped and perhaps correlated with related volcanic rocks [*White et al*., 2006; *Bachmann et al*., 2007]. The volumes of frozen intrusive bodies can be inferred from some combination of seismic, petrologic, and gravity data [e.g., *Farnetani et al*., 1996; *Korenaga et al*., 2002; *White et al*., 2006; *Leeman et al*., 2008; *Ridley and Richards*, 2010; *Richards et al*., 2013].

In spite of the uncertainties, some generalizations regarding Earth's *I/E* ratios seem robust. *White et al*. [2006] have compiled best estimates for the *I/E* ratios for 23 localities on Earth. Of these 23 localities, 20 have estimated *I/E* ratios of 10 or less. While *I/E* ratios can vary significantly, *White et al*. [2006] conclude that an *I/E* ratio of ~5 is a fair approximation for most magmatic systems. Although *White et al*. [2006] do not identify a clear relationship between tectonic setting and *I/E* ratio, detailed studies of arc and mid-ocean ridge magmatic systems underscore the importance of fractionation in arc systems [e.g., *Jagoutz and Schmidt*, 2012] and hint that compressional settings with thickened crust may favor larger *I/E* ratios. For example, large magma bodies have been inferred at depth beneath the Tibetan Plateau [*Brown et al*., 1996] and the Altiplano-Puna region of the central Andes [*Ward et al*., 2014]. The *I/E* ratio for the massive Altiplano-Puna magmatic system is approximately 20–35 over its 10 Myr history [*Ward et al*., 2014].

3. Intrusive/Extrusive Ratios on Mars

3.1. Sources of Uncertainty

On Mars, limited tools are available to estimate intrusive and extrusive volumes. Extrusive volumes must be estimated primarily from orbital mapping [e.g., *McEwen et al*., 1999; *Hiesinger and Head*, 2004; *Tanaka et al*., 2005]. In the absence of seismic data, remanent crustal magnetism provides one of the best records of intrusive activity [*Lillis et al*., 2009, 2015]. This approach considers the scale of intrusive magmatism required to heat the crust above the Curie temperature of magnetic minerals, thus removing remanent magnetization acquired when crustal rocks cooled through their Curie temperature in the presence of an ancient field. The major sources of uncertainty for this method are summarized in *Lillis et al*. [2015] and include the unknown thickness of the magnetized crustal rocks, the unknown magnetic mineralogy (the Curie temperature is ~670°C for hematite, 580°C for magnetite, and 330°C for pyrrhotite [*Dunlop and Özdemir*, 2001]), and the effects of saturation (a given rock can only be demagnetized once but may experience multiple episodes of intrusion and heating). Hydrothermal circulation around cooling intrusions has a small effect on thermal demagnetization [*Ogawa and Manga*, 2007].

Detailed studies of the crustal demagnetization in the Tharsis and Syrtis Major regions place constraints on the extent of intrusive magmatism at those locations [*Lillis et al*., 2009, 2015]. Temporally, the intrusions that caused thermal demagnetization must postdate the era of a dynamo-generated magnetic field, but the timing of intrusion since the cessation of the dynamo cannot be further resolved. The Argyre and Hellas impact basins lack crustal magnetic signatures, implying that the Martian dynamo had expired by the time these basins formed ~4.1 Ga [*Acuna et al*., 1999]. The intrusive volume estimates incorporated into the Tharsis and Syrtis Major *I/E* ratios discussed in the following sections may thus reflect cumulative magmatism that occurred at any time between ~4.1 Ga and the present. In addition, these estimates only reflect the volume of material intruded at depths less than that of the crustal Curie isotherm.

3.2. The Intrusive/Extrusive Ratio in the Tharsis Region

Tharsis is a vast volcanic province that encompasses ~20% of the surface area of Mars [e.g., *Solomon and Head*, 1982; *Lillis et al*., 2009]. The Mars Global Surveyor spacecraft carried an electron reflectometer instrument [*Acuna et al*., 1999] capable of measuring crustal magnetic fields exceeding a global detection limit of ~3 nT [*Lillis et al*., 2008b]. Crustal fields in a large region centered over Tharsis do not exceed this threshold, whereas nearby crustal fields can reach ~200 nT [*Lillis et al*., 2009]. Surface lava flows cannot plausibly explain the crustal heating required for thermal demagnetization [*Lillis et al*., 2009]. Modeling of stochastic sill and dike intrusion and crustal thermal evolution indicates that after the cessation of a Martian dynamo, 25–30 km of igneous intrusions would be sufficient to completely demagnetize the uppermost 30 km of the crust [*Lillis et al*., 2009]. In other words, the majority of the early, magnetized crust must be displaced and heated to remove the crustal field in the Tharsis region. *Lillis et al*. [2009] note that substantial thickening of the crust beneath Tharsis due to emplacement of intrusive material is consistent with inversions of gravity and topography, which show that crustal thickness may approach 100 km under Arsia Mons in the Tharsis province [*Neumann et al*., 2004]. The observed topography at Tharsis may also have implications for the *I/E* ratio. *Phillips et al*. [1990] developed an isostatic model for the support of Tharsis topography that indicates that *I/E* ratios may be 10–20, although a range of other models have been proposed to explain the topographic history of Tharsis [e.g., *Solomon and Head*, 1982; *Mège and Masson*, 1996a; *Phillips et al*., 2001; *Lowry and Zhong*, 2003].

The thermal demagnetization approach assumes that prior to magmatism the crust was magnetized to the depth of the Curie isotherm [*Lillis et al*., 2015]. Consequently, the thickness of the initial magnetized crust and the thickness of intruded rocks required to thermally demagnetize that crust both depend on the magnetic mineralogy. *Lillis et al*. [2009] find that if pyrrhotite is the magnetic carrier, ~10 km of intrusions were necessary, whereas if hematite is the magnetic carrier, ~35 km of intrusions were necessary. These thicknesses translate to intrusive volumes of $0.6–1.8 \times 10^6$ km^3 beneath the Arsia Mons volcano alone. Extrapolation of the mean thickness of the Arsia Mons rift apron to the entire area yields an upper bound on the extrusive volume in the Arsia Mons region of $\sim 2 \times 10^5$ km^3 [*Lillis et al*., 2009]. The 2500 km^3 volume of a field of small vents and flows east of Arsia Mons [*Bleacher et al*., 2009] constitutes a lower bound on the extrusive volume in the demagnetized region east of Arsia Mons [*Lillis et al*., 2009]. Accordingly, the lower bound on the *I/E* ratio in the vicinity of Arsia Mons is 3–10 and the upper bound is 250–750 [*Lillis et al*., 2009]. Even the lower bounds on the *I/E* ratio near Arsia Mons exceed estimated *I/E* ratios of 1–3 at the Hawaiian hot spot, although they fall within the overall range of *I/E* ratios on Earth [*White et al*., 2006; *Lillis et al*., 2009]. The upper bounds on the Arsia Mons *I/E* ratio are higher than any estimates for Earth in the compilation of *White et al*. [2006].

Lillis et al. [2009] calculated *I/E* ratios for the Arsia Mons region but not for Tharsis as a whole. However, it is possible to arrive at rough estimates, assuming that the 10–35 km thickness of intrusions required to demagnetize the Arsia Mons region [*Lillis et al*., 2009] holds for all of Tharsis. The approximate area of Tharsis is 3×10^7 km^2 [e.g., *Phillips et al*., 2001], implying intrusive volumes of $3–10 \times 10^8$ km^3. *Head et al*. [2002] combined mapping of buried Hesperian plains in the northern lowlands with the volume of Hesperian lavas in the Martian highlands to estimate a total Hesperian lava volume of $\sim 3.3 \times 10^7$ km^3. Late Noachian ridged plains cover a further 3% of the surface of Mars. Assuming a mean thickness of these Late Noachian lavas of 500 m to remain consistent with *Head et al*. [2002], the total volume of Late Noachian-Hesperian flood lavas is $\sim 3.5 \times 10^7$ km^3. If these lavas all originated from Tharsis and represent the bulk of the province's volcanic output, the implied *I/E* ratio is in the range of 9–29. Assuming a mean crustal thickness of 80 km in the Tharsis region [*Neumann et al*., 2004] yields a crustal volume of $\sim 2.4 \times 10^9$ km^3. If no intrusive material has been recycled into the mantle, the ratio of crustal volume to the volume of Late Noachian-Hesperian lavas represents an extreme upper limit on the *I/E* ratio at Tharsis of ~69.

Based on flood lava sequences up to 8 km thick exposed in the walls of the Valles Marineris canyon system, *McEwen et al*. [1999]estimated that the volume of extrusive rocks in the Valles Marineris region alone may reach $\sim 4 \times 10^7$ km^3 [*McEwen et al*., 1999]. If the volume of Tharsis volcanic rocks greatly exceeds $\sim 3.5 \times 10^7$ km^3, the Tharsis *I/E* ratio could be lower than we estimate here. The total volume of rock comprising the Tharsis load is $\sim 3 \times 10^8$ km^3 [*Phillips et al*., 2001], but much of this material may have been intrusive.

3.3. The Intrusive/Extrusive Ratio in the Syrtis Major Region

The Syrtis Major volcanic province is located just north of the Martian equator and just west of Isidis Basin, on the opposite side of the planet from Tharsis. The oldest volcanic activity at Syrtis Major occurred ~3.8–3.6 Ga, whereas the youngest volcanic activity occurred at 1.4–0.2 Ga [*Robbins et al*., 2011; *Lillis et al*., 2015].

Lillis et al. [2015] completed 4,725,000 stochastic intrusion simulations and found that intrusive replacement of ≥50% of the initially magnetized crust throughout the hourglass-shaped region of demagnetization yielded the best match with the observed crustal field at Syrtis Major. Depending on the magnetic mineralogy, implied estimates for intrusive volume at Syrtis Major are $4–19 \times 10^6$ km^3 [*Lillis et al*., 2015]. These volume estimates correspond to replacement of ~10–20 km of the preexisting magnetized crust. Geologic mapping of the Syrtis Major region found a total extrusive volume of $1.6–3.2 \times 10^5$ km^3 [*Hiesinger and Head*, 2004]. The *I*/*E* ratio at Syrtis Major is thus 12.5–120 (Table 1). This range of *I*/*E* values is higher than estimates for almost 90% of the localities surveyed by *White et al*. [2006] on Earth. A large positive gravity anomaly at Syrtis Major has been interpreted as evidence for solidified mafic cumulates [*Kiefer*, 2004; *Lillis et al*., 2015], consistent with the presence of a substantial volume of intrusive rocks.

3.4. Intrusive/Extrusive Ratios Elsewhere on Mars

In the absence of detailed magnetic or gravity studies as at Tharsis and Syrtis Major, the *I*/*E* ratio elsewhere on Mars remains poorly constrained. Tyrrhena Patera in the Martian highlands (located at ~21°S, 107°E) also shows a slightly negative magnetic anomaly. Because the demagnetization at Tyrrhena Patera is less extensive than at Syrtis Major and the volume of volcanic rocks is similar, *Lillis et al*. [2008b] suggested that the *I*/*E* ratio at Tyrrhena Patera might be lower than at Syrtis, but the precise value is uncertain.

By analogy with the Earth, *Greeley and Schneid* [1991] suggested a global Martian *I*/*E* ratio of 5–12. However, in light of the *I*/*E* estimates for Tharsis and Syrtis Major, the possibility of globally averaged *I*/*E* ratios outside this range should be considered. Comparison of the total volume of the Martian crust of $\sim 7200 \times 10^6$ km^3 [*Zuber*, 2001] with total estimated volcanic output of 68.8×10^6 km^3 [*Greeley and Schneid*, 1991] yields a crude upper limit on the global *I*/*E* ratio of ~100. However, much of the crustal volume may be ancient [*Elkins-Tanton et al*., 2005], and in many regions the crust retains a strong remanent magnetization [*Acuna et al*., 1999], implying that the true *I*/*E* ratio since the Noachian is much lower. As on Earth, the *I*/*E* ratio on Mars probably varies widely from location to location.

Remote sensing data, rover analyses, and shergottite meteorites constrain the composition of volcanic rocks on Mars. If these volcanic rocks represent the erupted fraction of the same magmas that crystallized to form intrusive rocks [*Bachmann et al*., 2007], and if fractionation of crystals from melt occurred prior to or during eruptions, the compositions of volcanic rocks should reveal the extent of this fractionation, thereby hinting at the mass of complementary intrusive material at depth. Fractionation of olivine from melt is expected to produce a gradual decline in the Mg content of the crystallizing olivine [*Roeder and Emslie*, 1970]. The bulk Mg numbers of basaltic shergottites range from 23 to 52, with MgO contents between 9.3 and 11.4 wt % [*Bridges and Warren*, 2006]. The bulk Mg numbers of Gusev crater basalts range from 51 to 55 [*McSween et al*., 2006]. In olivine-phyric shergottites, the composition of olivine ranges from Fo_{53} to Fo_{85} [*Bridges and Warren*, 2006; *Usui et al*., 2008]. For comparison, olivine crystallizing from Martian primary mantle melts is expected to be Fo_{74-85} [*Collinet et al*., 2015] and melt Mg numbers are expected to be 45–53 [*Baratoux et al*., 2011], depending on the temperature and therefore the degree of melting. Thus, the most primitive Martian volcanic rocks may represent relatively unmodified mantle melts [*McSween et al*., 2006; *Baratoux et al*., 2011; *Collinet et al*., 2015]. However, the presence of evolved dacitic rocks at Syrtis Major [*Christensen et al*., 2005; *Wray et al*., 2013], meteorite clasts with evolved compositions [*Humayun et al*., 2013; *Filiberto et al*., 2014], and the potassium enrichment in Jake_M [*Collinet et al*., 2015] provide evidence that other igneous rocks have experienced significant fractionation in the crust.

Atmospheric ^{40}Ar provides another perspective on the *I*/*E* ratio. Radiogenic decay of ^{40}K in the Martian mantle produces ^{40}Ar, which is strongly incompatible during melting [*Hutchins and Jakosky*, 1996; *Tajika and Sasaki*, 1996]. The accumulated ^{40}Ar in the present-day Martian atmosphere is thought to reflect the time-integrated history of mantle degassing from volcanism over the past ~4 Gyr [*Hutchins and Jakosky*, 1996; *Tajika and Sasaki*, 1996]. By assuming that 100% of magmatic ^{40}Ar degases, regardless of whether the host

magmas erupt, *Tajika and Sasaki* [1996] leverage the volcanic history of *Greeley and Schneid* [1991] to calculate the combined volume of intrusive and extrusive magmas required to release the presently observed ^{40}Ar inventory. They estimate a global *I*/*E* ratio on Mars of 56–167. The range reflects uncertainty in the extent of atmospheric loss due to sputtering or meteorites [*Jakosky and Jones*, 1997; *Brain and Jakosky*, 1998]. Because the upper bound is higher than our upper limit on the *I*/*E* ratio from the total volume of the Martian crust, it may be an overestimate. Results from the ongoing MAVEN mission may better constrain past atmospheric loss [*Jakosky et al*., 2015].

4. Methods

Several factors might lead to higher *I*/*E* ratios at Tharsis and Syrtis Major relative to most volcanic centers on Earth. Global thermal evolution [e.g., *Schubert et al*., 1993], mantle composition [e.g., *Dreibus and Wanke*, 1985], and tectonic regime [e.g., *Nimmo and Stevenson*, 2000] differ between Earth and Mars. We expect these global disparities to cause substantial differences in recharge rates, magma composition and volatile contents, lithospheric thickness and density structure, and regional stresses and strain rates at specific volcanic centers on Mars relative to their counterparts on Earth. In this study, we focus on evaluating the consequences of each of these factors for eruptibility at Tharsis, Syrtis Major, and elsewhere on Mars. While we consider each in turn, we note that in reality the controls on the *I*/*E* ratio likely reflect some combination of these factors.

To test the significance of recharge, we use scalings developed for magma chambers on Earth [*Dragoni and Magnanensi*, 1989; *Jellinek and DePaolo*, 2003; *Karlstrom and Richards*, 2011; *Caricchi et al*., 2014]. We combine these scalings with geologic and theoretical estimates of melt production on Mars and with constraints on crustal temperature during magmatism from the Curie temperatures of magnetic minerals to determine whether Tharsis and Syrtis Major magma bodies were in an elastic or viscous regime.

To test the significance of lithospheric properties and regional stresses, we compare stress magnitudes on Earth and Mars [*Zoback*, 1992; *Arkani-Hamed and Riendler*, 2002] and consider published constraints on the stress history of Tharsis and Syrtis Major [e.g., *Tanaka et al*., 1991; *Hiesinger and Head*, 2004]. We summarize observations and experimental results to gain perspective on the likely implications of strain rates.

Recharge and lithospheric stresses are most important when wall rocks are cold and stiff, preventing viscous relaxation. When the crust is warm, for example around the large magma volumes we expect from gravity [*Kiefer*, 2004] and demagnetization simulations [*Lillis et al*., 2009, 2015], buoyancy will dominate eruptibility [*Karlstrom and Richards*, 2011; *Caricchi et al*., 2014; *Malfait et al*., 2014]. We therefore require a model for buoyancy overpressure.

To test the importance of volatiles in Tharsis and Syrtis Major magmas, we employ a new one-dimensional model as described in Appendix A. One-dimensional models have often been used to study the thermal evolution of intrusions [e.g., *Annen and Sparks*, 2002; *Michaut and Jaupart*, 2006] because vertical length scales and gradients are much smaller and larger, respectively, than horizontal ones. In our model, we numerically solve the one-dimensional heat equation including the effects of latent heat. We map changes in temperature to changes in crystallinity and composition using a look-up table generated with MELTS [*Ghiorso and Sack*, 1995; *Gualda et al*., 2012]. In our MELTS calculations, we adopt a major element melt composition (Table 2) based on the parental melt for the basaltic shergottite meteorite EETA79001 [*Longhi and Pan*, 1989]. The fluid densities are calculated with a parameterized equation of state [*Degruyter and Huber*, 2014; *Halbach and Chatterjee*, 1982], and we combine the exsolved fluid density with melt and crystal densities from MELTS to obtain an overall magma density and thus the buoyancy overpressure (see equation (A9)). We assume that failure occurs at a critical chamber overpressure of 10 MPa, the approximate tensile strength of rock [*Rubin*, 1995].

Although recent work has shown that in reality large magma bodies often develop complex geometries with interconnected melt bodies spanning a range of depths [*Cashman and Giordano*, 2014; *Christopher et al*., 2015], here we consider an idealized geometry in which a single, laterally extensive magma body resides within the crust (Figure 1). We expect the thermal and compositional evolution of the magma in this idealized geometry to resemble that of a more complex geometry with multiple sills and dikes. However, because we allow bubbles to rise through the magma body and exit through permeable roof rocks, the fate of volatiles

Table 2. Initial Melt Composition as Calculated for the Composition of the Parental Melt for Meteorite EETA79001 Groundmass [*Longhi and Pan*, 1989; *Kress and Carmichael*, 1991; *Righter et al*., 2008], Initial Magma Temperature, And Critical Crystal Fraction [*Marsh*, 1981]

Oxide	Weight Percent
SiO_2	50.67
TiO_2	0.86
Al_2O_3	7.10
Cr_2O_3	0.12
FeO	16.06
Fe_2O_3	2.90
MgO	12.22
MnO	0.52
CaO	8.74
K_2O	0.07
Na_2O	1.07
Temperature (K)	1500
Critical crystal fraction	0.5

may differ from systems in which exsolving fluids are trapped at discrete levels until they amalgamate and escape during unrest or eruption [*Christopher et al*., 2015].

5. Results

5.1. Recharge

Magma bodies develop volume change overpressures as shifts in temperature, crystallization, and exsolution reduce magma density [*Tait et al*., 1989] and as fresh magma replenishes the magmatic system. The stresses surrounding an overpressured chamber will decay according to a Maxwellian viscoelastic relaxation time scale [*Dragoni and Magnanensi*, 1989; *Jellinek and DePaolo*, 2003; *Karlstrom and Richards*, 2011]:

$$\tau = \frac{\mu_{\text{crust}}}{E} \tag{1}$$

where μ_{crust} is the temperature-dependent wall rock viscosity (see equation (A12)) and E is the Young's modulus. For a spherical chamber the maximum chamber overpressure due to changes in magma volume (ΔP_{max}) can be formulated as [*Jellinek and DePaolo*, 2003]

$$\Delta P_{\text{max}} = \frac{2\mu_{\text{crust}} Q}{3V_{\text{ch}}} \tag{2}$$

where Q is the volumetric recharge and V_{ch} is the chamber volume. Ellipsoidal chambers reduce the overpressure needed for failure [*Currenti and Williams*, 2014].

If the maximum chamber overpressure for a given recharge rate, chamber volume, and wall rock viscosity is much larger than the overpressure required to cause failure and dike propagation, the wall rocks behave elastically. Conversely, if the maximum chamber overpressure is much lower than the critical overpressure, the magma chamber will be in a viscous regime where overpressures from volume change are efficiently relieved through viscous deformation (Figure 2). Following *Jellinek and dePaolo* [2003], we refer to these alternatives as the "elastic" and "viscous" regimes, respectively.

In the elastic regime on Earth, recharge is thought to be one of the major controls on whether magmas erupt [*Jellinek and DePaolo*, 2003; *Caricchi et al*., 2014], in conjunction with regional stresses [*McGovern et al*., 2015] and volume changes from crystallization and exsolution [*Tait et al*., 1989]. Figure 2 indicates that for smaller magma chambers located in cold, rigid crust, the rate of recharge will determine maximum chamber overpressure.

Melt production on Earth has been estimated at approximately 26–34 km^3/yr globally [*Crisp*, 1984]. At present, the majority of melting occurs at mid-ocean ridges (~18 km^3/yr [*Bird*, 2003]) and arcs (2.9–8.6 km^3/yr [*Crisp*, 1984]; *Jicha and Jagoutz* [2015] suggest that this range may underestimate magma production at intraoceanic arcs). Intraplate settings, including intermittent large igneous province eruptions [e.g., *Coffin and Eldholm*, 1994], contribute the remainder of magma production [*Crisp*, 1984].

In contrast to Earth, Mars lacks both spreading centers and arc volcanoes. Because of Mars' smaller size and absence of plate tectonics, its rates of melt production are likely to be lower than on Earth. From rates of surface volcanism [*Hartmann and Neukum*, 2001], *Kiefer* [2003] estimated global melt production during Mars' recent past of 1.5×10^{-4}–2×10^{-3} km^3/yr. This estimate assumes Earth-like *I*/*E* ratios [*Greeley and Schneid*, 1991; *Kiefer*, 2003]. A higher mean *I*/*E* ratio would imply higher rates of melt production in the Martian mantle, as discussed in section 6.2.

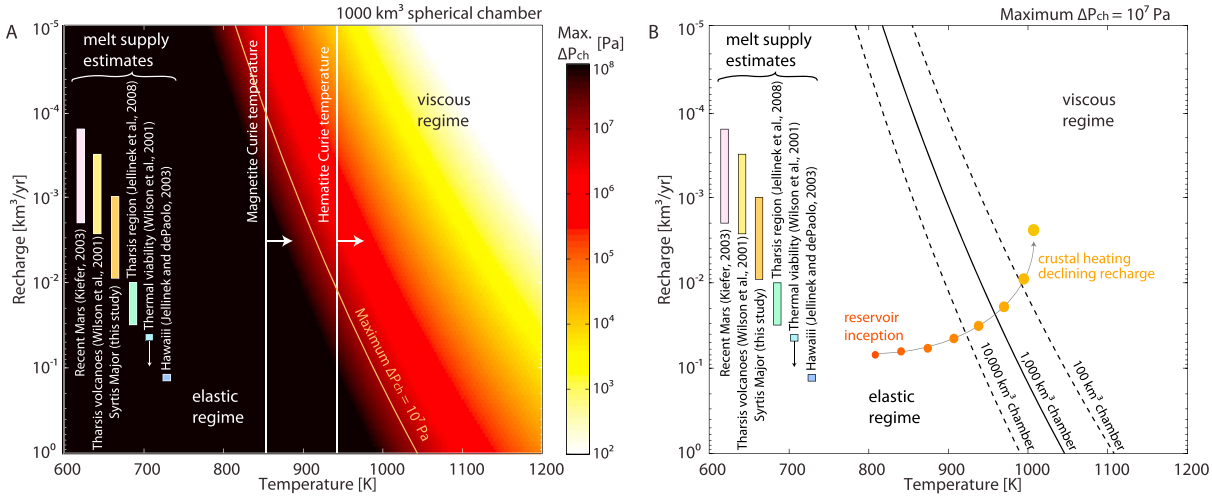

Figure 2. Controls on the maximum chamber overpressure for a spherical chamber and estimates of melt production on Mars. Melt supply estimates from *Wilson et al.* [2001] reflect time-averaged fluxes required to build individual Tharsis volcanoes and the minimum recharge required for magma chamber thermal viability. In all other cases, melt supply estimates reflect long-term averages, and the supply from the mantle may be divided among multiple magmatic systems and is therefore an upper limit on time-averaged recharge rates. (a) Recharge and wall rock temperature control the transition between elastic and viscous regimes in a 1000 km^3 magma body. Curie temperatures give a mineralogy-dependent lower limit on crustal temperatures attained during magmatism. (b) For a given recharge and wall rock rheology, chamber volume determines whether the maximum overpressure will be sufficient to cause eruption. See section 5.1 for details. Colored circles represent a conceptual trajectory for the evolution of a magmatic episode.

At Tharsis, *Jellinek et al.* [2008] estimate Noachian-Hesperian melt production of 0.01–0.03 km^3/yr. In section 6.2 we estimate somewhat higher rates of melt production at Tharsis of 0.08–0.25 km^3/yr averaged over 4 Gyr. Assuming growth over 1 Gyr, *Wilson et al.* [2001] estimate mean melt supply to individual Tharsis volcanoes of 4.1×10^{-4}–2.8×10^{-3} km^3/yr, similar to the estimated magma production rate at individual arc volcanoes on Earth [*Jicha and Jagoutz*, 2015]. *Isherwood et al.* [2013] obtain updated estimates of magma flux during the main phase of Olympus Mons activity of 3.0×10^{-3}–1.5×10^{-2} km^3/yr, and *Chadwick et al.* [2015] find that during the past 210 Myr Olympus Mons melt fluxes were in the range of 6.3×10^{-4}–6.4×10^{-3} km^3/yr.

At Syrtis Major, the volume of surface volcanism of $1.6–3.2\times10^5$ km^3 [*Hiesinger and Head*, 2004] combined with the volume of intrusions of $4–19\times10^6$ km^3 [*Lillis et al.*, 2015] gives cumulative melt production of $4.2–19.3\times10^6$ km^3 and time-averaged melt production over 2.2–3.6 Gyr [*Robbins et al.*, 2011] of $1–9\times10^{-3}$ km^3/yr.

It is challenging to infer recharge rates from time-averaged rates of melt supply from the mantle, for two reasons: (1) melt supply from the mantle may be distributed among multiple magmatic systems and is therefore an upper bound on time-averaged recharge rates and (2) recharge to magma chambers is likely unsteady and may have deviated significantly from time-averaged melt production and recharge. *Wilson et al.* [2001] suggest that thermal viability of magma reservoirs beneath the large Tharsis volcanoes required episodes with >0.03–0.3 km^3/yr recharge, much higher than time-averaged rates. During each magmatic episode, initially elevated rates of magma injection led to reservoir nucleation [*Wilson et al.*, 2001] and perhaps eruptions. Later in a magmatic episode, as the crust warmed, the reservoir grew, and recharge declined, we expect the system to transition toward a viscous regime in which recharge was less important for eruptibility (Figure 2b). Periods of weak recharge between magmatic episodes could have encouraged many magma bodies to freeze in the crust rather than erupting.

5.2. Regional Stresses and the Thickness and Density Structure of the Lithosphere

In this section, we discuss constraints on Martian crustal density structure, thickness, stresses, and strain rates, and we consider the implications for *I*/*E* ratios at Tharsis and Syrtis Major.

The density structure of the lithosphere controls the depth of neutral buoyancy [*Wilson and Head*, 1994]. *Wilson and Head* [1994] suggest that impact brecciation of the uppermost crust (Figure 1) leads to an increase

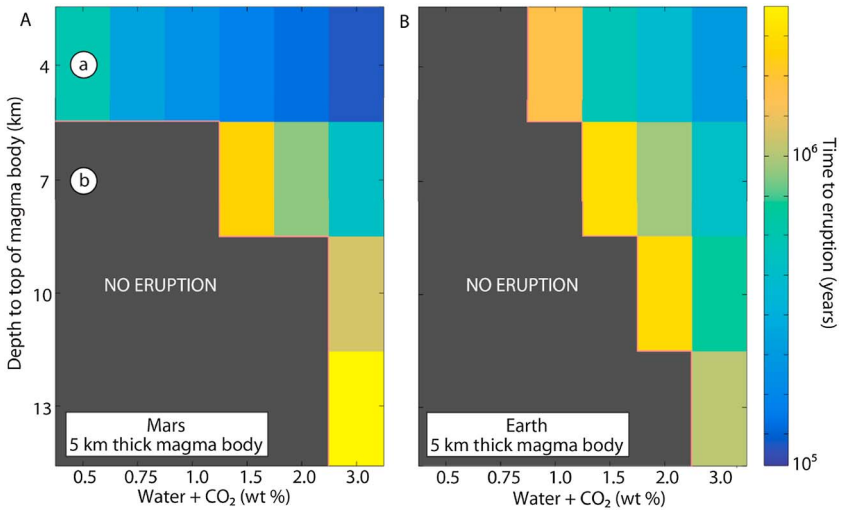

Figure 3. Time until eruption as a function of depth and initial volatile contents for (a) Mars gravity and (b) Earth gravity in the viscous regime. The initial depth-permeability profile on Mars is rescaled from *Manning and Ingebritsen* [1999] for lower Martian gravity by assuming that depth can be converted to pressure. Simulations assume a 5 km thick magma chamber (chamber depth is given for the top of the chamber) with negligible recharge. Higher gravity on Earth accelerates porosity loss, trapping exsolved volatiles in the chamber. However, at shallow depths this effect is strongly offset by lower volatile density. Lowercase "a" and "b" denote the simulations shown in Figures 4a and 4b, respectively.

in porosity and a decrease in density, potentially causing basaltic magmas to stagnate at depths of ~11 km. Under higher lithostatic pressure, the density of a coexisting volatile phase is also higher, and exsolving volatiles contribute less buoyancy. Therefore, once a magma stalls at middle to lower crustal depths, buoyancy from volatile exsolution is unlikely to cause eventual eruption unless initial volatile concentrations were high (see discussion in the following section). We illustrate this conclusion in Figure 3, in which we use the model described in Appendix A to calculate buoyancy overpressure within a slowly freezing magma body.

The thickness of the lithosphere can influence the pressure and extent of partial melting and thus the composition and density of magmas [*Ridley and Richards*, 2010; *Baratoux et al*., 2011, 2013]. Greater crustal thickness should also allow more energy loss during ascent, thereby increasing the likelihood a magma will freeze rather than erupting [*Shaw*, 1980; *Huppert and Sparks*, 1985; *White et al*., 2006]. The crust in the Tharsis region reaches thicknesses of ~100 km, which exceeds crustal thicknesses anywhere else on Mars [*Neumann et al*., 2004]. However, the thickness of the crust beneath Tharsis may in part be a consequence rather than a cause of intense intrusive activity [*Phillips et al*., 1990; *Lillis et al*., 2015]. A large positive gravity anomaly beneath Syrtis Major has been interpreted as either an upwarped Moho or as the signature of an immense volume of dense, frozen magma [*Neumann et al*., 2004; *Kiefer*, 2004; *Lillis et al*., 2015]. Crustal thickness immediately adjacent to Syrtis Major is approximately 55 km [*Neumann et al*., 2004], greater than the typical 30–40 km thickness of continental crust on Earth but less than the ~75 km thickness of the crust beneath Tibet, which is presently the thickest crust on Earth [*Rudnick*, 1995; *Rudnick and Fountain*, 1995].

Earth has plate tectonics, whereas Mars does not, at least not at present [*Nimmo and Stevenson*, 2000]. Topographic loading on Mars can produce stresses that are similar in magnitude to tectonic stresses on Earth [*Arkani-Hamed and Riendler*, 2002; *Zoback*, 1992]. The Syrtis Major and Tharsis regions have apparently experienced both extension and compression, perhaps due in part to mantle dynamics or the development of the magmatic plumbing system and edifice [e.g., *Willemann and Turcotte*, 1982; *Sleep and Phillips*, 1985; *Phillips et al*., 1990; *Watters*, 1993; *Tanaka et al*., 1991; *Mège and Masson*, 1996b; *Hiesinger and Head*, 2004]. The orientation of caldera features relative to flank structures suggests that regional stress fields may have influenced volcanic eruptions [*Crumpler et al*., 1996]. Some rift structures may also have developed above ascending dikes [*Scott et al*., 2002; *Wilson and Head*, 2002].

In contrast to the similar regional stress magnitudes on Earth and Mars, typical strain rates may be very different. Plate tectonics on Earth leads to high strain rates at plate boundaries of 10^{-15}–10^{-14} s^{-1} [e.g., *Jackson and McKenzie*, 1988; *Tikoff and Teyssier*, 1994]. While crustal strain rates on Mars are poorly constrained, in the absence of plate tectonics they are thought to be generally much lower [*McGovern et al*., 2002; *Grott and Breuer*, 2008].

The overall consequences of diminished strain rates for the *I*/*E* ratio are not obvious. In regions of extension such as rifts and spreading centers, high tectonic strain rates can create space for ascending dikes [e.g., *Daniels and Menand*, 2015], which might increase the *I*/*E* ratio if most magma is emplaced in the crust. The estimated *I*/*E* ratios at the East Pacific Rise and the Mid-Atlantic Ridge are both higher than at Hawaii [*White et al*., 2006], indicating that in extensional settings high strain rates could act to increase the *I*/*E* ratio. In regions of compression, increased crustal thickness should favor a higher *I*/*E* ratio for the reasons discussed above, but compression might also help to pressurize the magmatic system, encouraging eruption to the surface [*Rubin*, 1995]. On the other hand, in highly compressive settings less space may be available for magmas to ascend from the mantle into the crust. However, experiments show that ascending dikes can rotate to form sills that thicken the crust when compression is very strong or when buoyancy is weak [*Menand et al*., 2010]. These competing effects of tectonic setting and strain rates may explain the contradictory and inconclusive relationship between these factors and the *I*/*E* ratio in existing global compilations for Earth [*Crisp*, 1984; *White et al*., 2006].

In summary, lithospheric density, thickness, and regional stresses and strain rates have clearly affected the expression of magmatism at Tharsis, Syrtis Major, and elsewhere on Mars. However, variations in regional stresses and strain rates can exert conflicting influences on eruptibility, suggesting that the clear differences in tectonic histories on Earth and Mars might not carry straightforward manifestations in magmatic *I*/*E* ratios.

5.3. Volatiles in a Warm Crust

For large magma bodies with slow recharge in warm crust, the magmatic system will be in the viscous regime, and eruptibility will be controlled by buoyancy. Unlike volume change overpressures and regional stresses, deviatoric stresses due to buoyancy overpressure do not relax viscoelastically [*Karlstrom et al*., 2010; *Degruyter and Huber*, 2014; *Caricchi et al*., 2014]; buoyancy overpressure is only alleviated through volatile escape or roof failure [*de Silva and Gregg*, 2014].

The density of mafic melts changes slowly up to large degrees of fractionation (when crystallization of oxides leads to rapidly declining melt density) [*Cox*, 1980]. In our MELTS simulations, 50% crystallization of the initial melt leads to a density increase of ~3–5% (depending on crystallization pressure). Therefore, for mafic magmas volatiles exert a dominant control on buoyancy. Mafic magmas will only erupt due to buoyancy overpressure when sufficient quantities of volatiles exsolve and when exsolution outpaces permeable escape of volatiles. Volatile exsolution reduces the overall density of a bubbly magma and therefore increases the likelihood of eruption [*Tait et al*., 1989; *Karlstrom and Richards*, 2011]. During decompression, water exsolution can lead to an increase in liquidus temperatures and consequently to crystallization and pluton formation [*Couch et al*., 2003]. However, in a stalled and slowly crystallizing magma body (such as we envision in our model), volatile exsolution results from crystallization rather than decompression. On balance, magmas that contain limited volatile budgets should therefore contribute to a higher *I*/*E* ratio. Although Martian magmas may be very sulfur rich, we expect water and CO_2 to be most relevant to eruptibility.

We consider the development of buoyancy overpressure with a one-dimensional model that tracks magmatic volatiles (described in detail in Appendix A). Here we assume that magmas are initially saturated in water and CO_2. If highly reducing conditions prevail in the Martian mantle and melt CO_2 concentrations in equilibrium with the mantle are very low [*Hirschmann and Withers*, 2008], ascending magmas may be volatile undersaturated, which would further suppress buoyant eruptibility. Volatile exsolution can also lead to deviatoric stresses due to changes in chamber volume [*Tait et al*., 1989], but in the viscous regime these stresses will relax just as stresses from replenishment do, and therefore, we neglect this effect in our model.

We conduct a series of one-dimensional simulations of magmatic systems that account for volatile escape and the rise and coalescence of bubbles, and we find that bubbles rise efficiently to the top of the magmatic system, and the initial volatile escape quickly alleviates buoyancy overpressure (Figure 4). Volatile egress from magma chambers depends on the permeability of the surrounding rocks, which in turn reflects the interplay

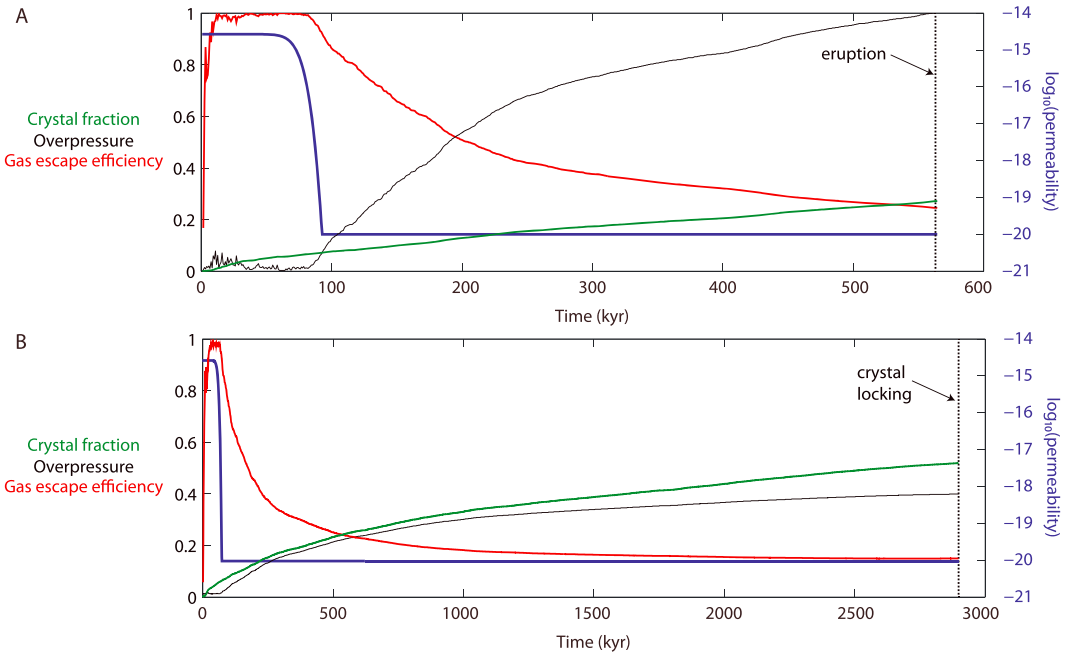

Figure 4. Gas escape efficiency (red curves; the fraction of total cumulative exsolved fluid that has exited the magma chamber), overpressure (black curves, normalized to 10 MPa), and crystal fraction (green curves) for (a) a chamber that erupts and (b) a chamber that freezes (these particular simulations are marked "a" and "b," respectively, in Figure 3). Blue lines (right axes) show the permeability evolution in the overlying country rock. We impose a minimum permeability of 10^{-20} m^2, based on the lowest permeability observed in metamorphic rocks on Earth [*Manning and Ingebritsen*, 1999].

of temperature-dependent ductile creep and fracturing due to elevated pore pressures [*Weis et al*., 2012]. In our model we account for viscous compaction, but we only allow fracture-induced increases in permeability during eruptions, when overpressure leads to failure of the country rocks surrounding the magma. Consequently, after the simulated magma bodies heat the wall rocks, viscous compaction progressively diminishes wall rock permeability, trapping the majority of volatiles within the magma body and allowing overpressure to build toward the eruption threshold.

The characteristic time scale for viscous compaction (as formulated in equation (A11)) is $\tau_c = \frac{\mu_{crust}}{\rho g h}$, where $\rho g h$ is the lithostatic pressure. The viscosity of the crust μ_{crust} will depend on temperature at a given distance L from an intrusion (equation (A12)). The thermal diffusion time scale is $\tau_t = \frac{L^2}{\kappa}$, where κ is the thermal diffusivity. If we assume that the crust must be warm for several hundred meters around the magma body to seal in volatiles, for $\kappa = 5 \times 10^{-7}$ m^2/s, the thermal diffusion time scale is ~10^4 years. Figure 4 confirms that in our simulations viscous compaction and porosity loss occur on time scales of ~10^4–10^5 years. The initial permeability profile we assume is rescaled from Earth [*Manning and Ingebritsen*, 1999] and may in reality differ significantly for Mars [*Clifford*, 1993; *Clifford and Parker*, 2001]. However, magmatic systems that last more than 10^5 years will effectively overprint the crustal porosity and permeability in their vicinity. If hydrofracturing is pervasive, as models [*Weis et al*., 2012] and field studies [*Gruen et al*., 2010] suggest it is around hydrous magma bodies on Earth, it would further enhance magmatic overprinting of crustal porosity and permeability. On the other hand, if Martian magmas are relatively volatile poor, we expect hydrofracturing to be less significant.

In Figure 5, we consider the end-member case in which all bubbles rise to the top of the magma body and no volatiles escape from the magma, and we determine the minimum volatile contents required to trigger an eruption through buoyancy alone (equation (A16)). Extensive hydrofracturing would expedite volatile egress from the magma reservoir, implying that this end-member scenario may underestimate the volatile contents required for eruption. Nevertheless, with these assumptions, and for uniform distributions of the depth and size of the magma body, it is possible to calculate the expected *I*/*E* ratio as a function of the magmatic volatile budget (Figure 5).

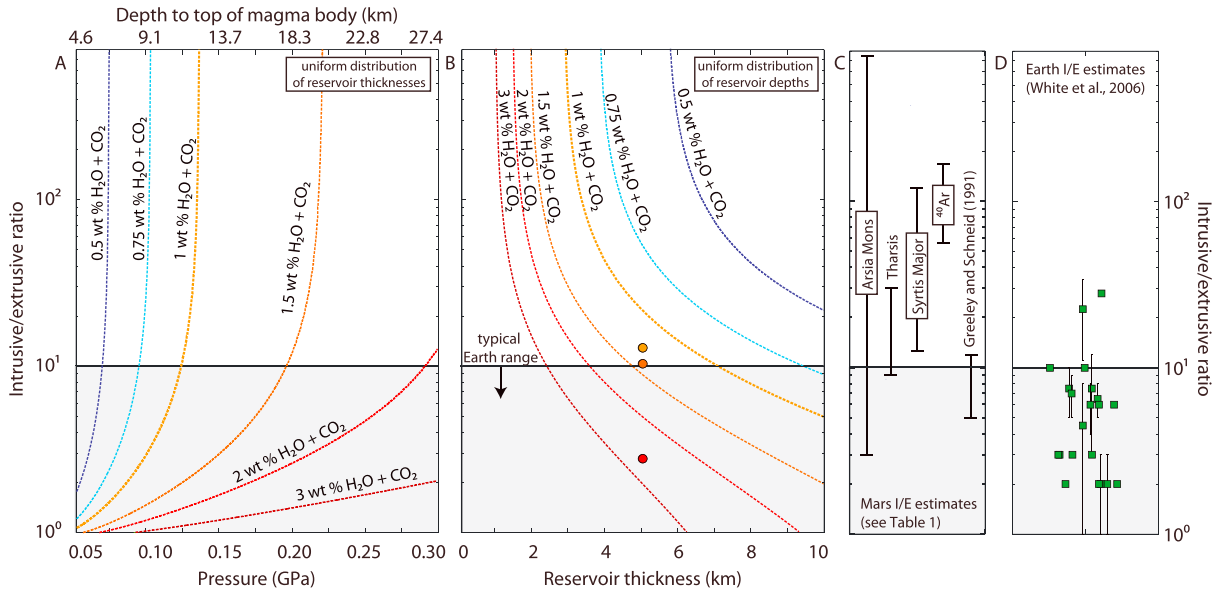

Figure 5. Intrusive/extrusive ratios on Mars as a function of initial volatile contents. Curves are computed with equation (A16): (a) for a given volatile content and chamber depth, assuming a uniform distribution of chamber thicknesses (between 0.1 and 10 km), and (b) for a given volatile content and chamber thickness, assuming a uniform distribution of chamber depths (between 0.05 and 0.30 GPa, which on Mars correspond to depths of approximately 5 and 27 km, respectively). Colored circles correspond to the intrusive/extrusive ratio calculated from the full set of simulations shown in Figure 3 (which account for gas escape, bubble rise, and eruption prior to the critical crystal fraction) with a uniform depth distribution, a 5 km thick chamber, and variable volatile contents. (c) Intrusive/extrusive ratios on Mars from published estimates (see Table 1 for details and references). (d) Intrusive/extrusive ratios on Earth, from *White et al.* [2006]. In Figures 5c and 5d, the *I/E* ratios are spread along the horizontal axis to increase legibility.

For magmas in the viscous regime, we expect that low mean volatile contents, deep-seated magmatic systems, thin isolated magma bodies, or some combination of these factors could reproduce the observed range of *I/E* ratios at Tharsis and Syrtis Major (Figure 5).

6. Discussion and Implications

6.1. Causes of Suppressed Eruptibility at Tharsis and Syrtis Major

Building on the work of *Wilson et al.* [2001], we envision a cyclical history of Tharsis and Syrtis Major magmatism characterized by episodes of elevated recharge separated by long periods of quiescence. Throughout each phase of this magmatic history, our analysis suggests that several factors may have influenced eruptibility. During the early stages of a magmatic episode when recharge was high and the crust was elastic, we expect the likelihood of eruption to be greatest.

After this initial period of each magmatic episode, minimum recharge rates are lower [*Wilson et al.*, 2001]. However, the presence of large quantities of newly arrived magma should have warmed the crust, offering a possible explanation for the observed demagnetization [*Lillis et al.*, 2008a, 2009, 2015]. If pyrrhotite is the dominant magnetic mineral, only modest heating was required to demagnetize the crust at Tharsis and Syrtis Major. However, if magnetite or hematite carried the remanent magnetization, the requisite heating (to greater than 580°C or 670°C, respectively [*Dunlop and Özdemir*, 2001]) may have been sufficient to shift the crust into a viscous regime (Figure 2), in which thermally activated creep relieved stresses and overpressures due to replenishment and regional tectonics. Waning recharge and growing magma reservoirs (supported by the estimated volumes of Tharsis and Syrtis Major calderas [*Crumpler et al.*, 1996] and flood lavas [*Carr et al.*, 1977; *Wilson et al.*, 2001]) would further favor a viscous regime (Figure 2b).

Even during this waning phase of each magmatic episode, sufficient buoyancy from volatile exsolution could still cause eruptions [*Malfait et al.*, 2014; *Caricchi et al.*, 2014; *Degruyter and Huber*, 2014]. The elevated *I/E* ratios at Tharsis and Syrtis Major thus imply that most of these magmas were too volatile poor to erupt through buoyancy overpressure alone. Our model demonstrates that initial water and CO_2 contents typically

<1.5 wt % can reproduce the observed range of *I/E* ratios during periods when the crust was warm or recharge was weak.

6.2. *I/E* Ratios and Tharsis Melt Production

From published estimates of the volume of volcanic rocks at Tharsis, we can use the *I/E* ratio to predict total melt production from a hypothesized mantle plume [e.g., *Li and Kiefer*, 2007]. As in section 3.2, we consider an extrusive volume equivalent to the estimated Late Noachian-Hesperian lava volume of ~3.5×10^7 km^3 [*Head et al*., 2002]. For this volume, an Earth-based *I/E* ratio of 5–12 [*Greeley and Schneid*, 1991] implies cumulative Tharsis melt production of 0.2–0.4 $\times 10^9$ km^3 and a time-averaged melt production over the past 4 Gyr of 0.05–0.1 km^3/yr. If Tharsis was largely emplaced during the first billion years of Martian history [*Phillips et al*., 2001], melt production during that time was 0.2–0.4 km^3/yr, significantly higher than predicted from mantle convection modeling [*Jellinek et al*., 2008].

Applying Tharsis *I/E* ratios of 9–29 as discussed in section 3.2 increases expected melt production to 0.3–1.0 $\times 10^9$ km^3. Averaged over 4 Gyr, this equates to 0.08–0.25 km^3/yr; averaged over 1 Gyr, it equates to 0.3–1.0 km^3/yr. If correct, the upper estimates suggest that Late Noachian-Hesperian melt production at Tharsis could have approached recent intraplate melt production on Earth [*Crisp*, 1984]. The lower estimates are comparable to estimated melt production of ~0.15 km^3/yr at Hawaii [e.g., *Jellinek and DePaolo*, 2003], the most prolific hot spot on Earth. These revised estimates of Tharsis melt production may serve as useful constraints for models of Martian thermal evolution [e.g., *O'Neill et al*., 2007; *Li and Kiefer*, 2007; *Jellinek et al*., 2008; *Šrámek and Zhong*, 2012; *Sekhar and King*, 2014] and also carry implications for volatile outgassing.

6.3. Implications of Magmatic Volatile Contents for Degassing From Tharsis and Syrtis Major

Massive CO_2 degassing from Tharsis has been invoked to explain the relatively warm climate necessary for Martian surface hydrologic activity [*Phillips et al*., 2001]. Alternatively, greenhouse effects from volcanogenic SO_2 may also be capable of supporting brief intervals with surface temperatures above 273 K [*Halevy and Head*, 2014]. Three quantities determine the magnitude of volatile outgassing during magmatism: the total mass of melt, the concentration of volatiles in the melt, and the fraction of those volatiles that are released to the atmosphere.

From our simulations of magmatic eruptibility when the crust is warm, we infer that Tharsis and Syrtis Major magmas carried limited quantities of water and CO_2. This conclusion agrees with constraints on volatile concentrations in Martian magmas from SNC meteorites and thermodynamic calculations. Measurements of water concentrations in shergottite melt inclusions [*Usui et al*., 2012] are consistent with a relatively water poor Martian mantle [*Dreibus and Wanke*, 1985; *Mysen et al*., 1998], although water concentrations in apatite indicate that at least some source regions may contain up to several hundreds of parts per million of water [*McCubbin et al*., 2010]. Carbon partitioning during melting depends strongly on oxygen fugacity. Trace element oxybarometers suggest that the Martian mantle is much more reducing than Earth's mantle [*Wadhwa*, 2001; *Righter et al*., 2008]. Consequently, graphite and diamond are expected to be the stable carbon-bearing phases [*Hirschmann and Withers*, 2008], and low-degree melts will be relatively carbon poor [*Hirschmann and Withers*, 2008; *Stanley et al*., 2011]. At 1350°C, with oxygen fugacity at or slightly above the Fe-FeO buffer, basalts can dissolve 51–665 ppm C at 1.2 GPa [*Stanley et al*., 2011; *Wetzel et al*., 2013].

In contrast to water and CO_2, Martian magmas are likely sulfur rich [e.g., *Johnson et al*., 2008; *Righter et al*., 2009], which may not contribute significantly to eruptibility but is important for outgassing [*Gaillard and Scaillet*, 2009]. Outgassing is often estimated based on extrusive volume [e.g., *O'Neill et al*., 2007], but silicic eruptions on Earth commonly release excess gas derived from intrusive residues [*Keppler*, 1999; *Shinohara*, 2008]. If substantial intrusive bodies contributed excess sulfur during the eruption of felsic rocks at Syrtis Major [*Christensen et al*., 2005; *Wray et al*., 2013] they may have expelled larger than expected quantities of sulfur.

7. Conclusions

Intrusive magmatism has been hypothesized to explain demagnetization of large regions of crust in the Tharsis and Syrtis Major regions [*Lillis et al*., 2009; *Lillis et al*., 2015]. Comparison with volumes of extrusive rocks suggests that the majority of Tharsis and Syrtis Major magmas froze in the subsurface, and indeed that

the *I/E* ratio at Tharsis and Syrtis Major may be higher than at most volcanic centers on Earth [*White et al*., 2006], with implications for estimation of cumulative melt production and volatile outgassing.

To assess why intrusive magmatism is so prevalent at Tharsis and Syrtis Major, we consider the role of recharge, lithospheric properties, regional stresses and strain rates, and volatile budget. We conclude that the thick crust, spasmodic magma replenishment, crustal heating, and limited quantities of magmatic water and CO_2 [*Dreibus and Wanke*, 1985; *Mysen et al*., 1998; *Hirschmann and Withers*, 2008; *Stanley et al*., 2011; *Usui et al*., 2012] are among the most important factors in the suppressed eruptibility of Tharsis and Syrtis Major magmas. A limited water and CO_2 budget in most Martian magmas implies that SO_2 or other greenhouse gases are required to link volcanism to clement surface temperatures on early Mars [*Hirschmann and Withers*, 2008; *Halevy and Head*, 2014].

Appendix A: Eruptibility in the Viscous Regime

A1. Model Overview

If viscous relaxation efficiently relieves deviatoric stresses around a magma body, buoyancy will control eruptibility. To evaluate the conditions under which buoyancy will or will not cause Martian magmatic systems to erupt, we employ a one-dimensional model that combines thermal evolution (as detailed in section A2), bubble coalescence and rise (as detailed in section A4), and viscous compaction and permeable gas escape (as detailed in section A6). We solve the one-dimensional heat equation with latent heat numerically. To relate changes in magmatic enthalpy due to heat transfer to changes in temperature, crystallinity, density, and liquid viscosity we use a thermodynamic look-up table computed with MELTS [*Ghiorso and Sack*, 1995; *Gualda et al*., 2012]. Crystallinity strongly influences magma viscosity [*Marsh*, 1981]. We use the Einstein-Roscoe relationship [*Marsh*, 1981] to calculate magma viscosity from melt viscosity and crystallinity (see section A4).

We assume an initial major element melt composition (see Table 2) based on the parental melt for the basaltic shergottite meteorite EETA79001 [*Longhi and Pan*, 1989] and consider a range of initial volatile concentrations. We focus on buoyancy from exsolution of magmatic water and CO_2, because sulfur species do not consistently exsolve until shallow depths [*Dixon et al*., 1991]. The solubility of both water and CO_2 increase with increasing pressure; higher dissolved CO_2 reduces water solubility and vice versa [*Dixon and Stolper*, 1995].

Exsolved fluids initially escape through the surrounding country rock, but as the wall rock warms, viscous compaction accelerates and permeability declines, trapping volatiles in the magma body. When the resulting buoyancy overpressures surpass 10 MPa [*Rubin*, 1995], we assume that there is an eruption. We further assume that once an eruption begins, a siphoning effect [*Karlstrom and Manga*, 2009; *Karlstrom et al*., 2012] draws out the melt from the magmatic system, leaving behind the crystal fraction. If crystallinity in the chamber reaches 50% we consider the magma locked and uneruptible [*Marsh*, 1981]. This assumption contrasts with counterexamples on Earth where crystal-rich magmas do in fact erupt [e.g., *Huber et al*., 2012].

In our model, we do not explicitly consider fracturing and dike propagation [*Rubin*, 1995] nor do we consider elastic stresses. Eruptibility in an elastic regime is discussed in section 4.

A2. Thermal Evolution Model

In our one-dimensional model, we consider only conductive heat transfer in the vertical direction. The 1-D heat equation with latent heat is [e.g., *Huber et al*., 2009]

$$\frac{dT}{dt} = \frac{L}{c_p}\frac{dF_{\mathrm{xtal}}}{dt} - \kappa \nabla^2 T \tag{A1}$$

Here T is the temperature, κ is the constant thermal diffusivity, and f_{xtal} is the crystal fraction. In the country rock, we calculate the temperature directly from the heat capacity and density of the rock ($c_{p,\mathrm{crust}}$ and ρ_{crust}, respectively). In the magma body, to account for the latent heat of crystallization we use a look-up table generated with MELTS [*Ghiorso and Sack*, 1995; *Gualda et al*., 2012] to interpolate to the temperature at a given enthalpy.

This look-up table approach allows us to incorporate the rigor of MELTS without simplifying thermodynamic relationships. However, it implicitly assumes batch crystallization with a fixed bulk magma composition (see Table 2). The thermodynamic calculations also assume a fixed initial volatile composition, irrespective of the range in volatile contents we consider for the eruptibility calculations described below.

A3. Volatile Exsolution

The solubility of water (as a function of CO_2 contents) and CO_2 (as a function of water contents) can be computed for a given pressure with VolatileCalc [*Newman and Lowenstern*, 2002]. However, the relative proportions and overall concentrations of water and CO_2 in Martian magmas are poorly constrained. For a given magma depth and pressure, we therefore assume that magmas are initially saturated in water and CO_2, and we consider a range of total water and CO_2 contents (corresponding to a range in water/CO_2 ratios) that satisfy this pressure-dependent saturation condition. As crystallization proceeds, water and CO_2 exsolve, thereby lowering the overall magma density. We do not account for any thermodynamic feedback due to volatile exsolution and escape nor do we consider hydrous fractionation.

If water and CO_2 are initially undersaturated in some Martian magmas, exsolution will be delayed until fractionation and/or decompression cause the magma to reach saturation. Thus, volatile undersaturated magmas, like volatile-poor magmas, would suppress the eruptibility (and increase the *I*/*E* ratio) of Martian magmatic systems.

A4. Bubble Coalescence and Rise Model

Bubble coalescence matters because the volatile phase is compressible, and therefore, its density is lower if it reaches the top of the magma body. Efficient segregation of volatiles toward the top of the magma body will increase buoyancy. Bubble rise speeds, U_s, due to buoyancy depend on bubble radius, a:

$$U_s = \frac{2(1+\lambda)\Delta\rho g\, a^2}{3(2+3\lambda)\mu_{\text{magma}}} \tag{A2}$$

where λ is the viscosity of the bubble divided by the viscosity of the surrounding magma, μ_{magma}. For exsolved volatiles within a magma, λ approaches zero, and equation (2) reduces to

$$U_s = \frac{\Delta\rho g\, a^2}{3\mu_{\text{magma}}} \tag{A3}$$

where $\Delta\rho$ is the density contrast between a bubble and the melt. The viscosity of the magma depends on its crystallinity, f_{xtal}, and can be calculated from the melt viscosity μ_{melt} with the Einstein-Roscoe relationship [*Marsh*, 1981]:

$$\mu_{\text{magma}} = \mu_{\text{melt}}\left(\frac{f_{\text{xtal, max}}}{f_{\text{xtal, max}} - f_{\text{xtal}}}\right)^{2.5} \tag{A4}$$

We retrieve μ_{melt} and f_{xtal} from our MELTS look-up table. The critical crystal fraction for locking $f_{\text{xtal,max}}$ is typically taken to be $f_{\text{xtal,max}}$~0.5–0.65 [*Marsh*, 1981; *Huber et al*., 2011]. Here we assume that $f_{\text{xtal,max}} = 0.5$. The ascent of bubbles in a magma will depend on the abundance and size of both bubbles and crystals [*Belien et al*., 2010]. For a bubbly melt with few crystals, the melt viscosity and magma viscosity in our formulation converge, and it is this viscosity that resists bubble ascent. For very crystal rich magma, fluids may travel through permeable pathways [*Burton et al*., 2007]. In regimes between these end-members, bubble behavior may be more complex. For example, in crystal-rich suspensions with small bubbles, crystals are largely immobile, bubbles must deform to move between the crystals, and melt viscosity resists bubble motion [*Belien et al*., 2010]. Our model applies to systems with bubble migration but not to crystal-rich systems, in which we assume that bubble migration effectively ceases.

The size distribution of the bubbles at each depth in the magma evolves as bubbles coalesce. Following *Manga and Stone* [1995], we bin the bubble population into N bins according to bubble radius and model the population dynamics as

$$\frac{dN_k}{dt} = \frac{1}{2}\sum_{i+j=k} J_{ij} - \sum_{i=1} J_{ik} \tag{A5}$$

where the change in the number of bubbles in a given size bin N_k per unit volume per time is defined by the balance between coalescence of two smaller bubbles to form a bubble of that size (the left-hand term) versus the loss of bubbles from a bin as they grow larger (the right-hand term). The collision frequency function J_{ij}, which describes the number of collisions per unit volume between bubbles in bin i and bin j, depends on the number of bubbles in each bin (N_i and N_j, respectively), their rise velocities ($U_{s,i}$ and $U_{s,j}$, respectively), and their capture cross section y_c^2:

$$J_{ij} = N_i N_j \pi \left(U_{s,i} - U_{s,j}\right) y_c^2. \tag{A6}$$

Experimental results [*Manga and Stone*, 1995] suggest that the capture cross section can be represented with the following empirical formula:

$$y_c^2 = \left(a_i + a_j\right)^2 \times \left[0.3\sqrt{\frac{a_i}{a_j}} + \frac{1}{2}B\left(\frac{v_j}{v_i}\right)^2\right] \tag{A7}$$

where $B = \Delta\rho g\, a^2/\sigma$ is the Bond number and v_i and v_j are the volumes of the smaller and larger coalescing bubbles, respectively. This empirical relationship is consistent with theoretical results for spherical bubbles when B approaches zero [*Zhang and Davis*, 1991]. We assume that the efficiency of collisions is 100% (i.e., all collisions result in bubble mergers).

The density of an exsolved fluid or gas phase depends on pressure and temperature. As bubbles rise to successively shallower depths in the magma, we recalculate their density (in kg/m^3) according to a parameterized Redlich-Kwong equation of state [*Degruyter and Huber*, 2014; *Halbach and Chatterjee*, 1982]:

$$\rho_{\text{gas}} = -112,528\, T^{-0.381} + 127,811\, P^{-1.135} + 112,040\, T^{-0.411}\, P^{0.033} \tag{A8}$$

where temperature T is in units of kelvin and pressure P is in units of bars. We use this fluid density to calculate the overall magma density.

A5. Buoyancy Overpressure

As volatiles exsolve, their presence decreases the density of the bubble-bearing magma. This diminished density creates a buoyancy overpressure that can only be relieved if the volatile phase escapes [e.g., *Blake*, 1984; *Karlstrom and Richards*, 2011; *Malfait et al.*, 2014].

The density of the magma, ρ_{magma}, is simply the sum of the gas, melt, and crystal masses divided by the sum of the volumes occupied by each phase. We then calculate the buoyancy-related magma overpressure (ΔP_b) as

$$\Delta P_b = \left(\rho_{\text{surrounding}} - \rho_{\text{magma}}\right) g\, h \tag{A9}$$

where h is the thickness of the magma body in meters, $g = 3.71$ m/s^2 is the Martian gravitational acceleration, and we assume that the magma has ascended to a level of neutral buoyancy and that therefore the density of the country rocks at that depth ($\rho_{\text{surrounding}}$) is identical to the initial density of the magma (ρ_{magma}).

A6. Porosity-Permeability Model

Percolation theory provides an idealized relationship between porosity, ϕ, and permeability, k:

$$\kappa = c(\phi - \phi_{cr})^{\mu_p} \tag{A10}$$

where c and μ_p are the constants [*Sahimi*, 1994]. For fractured and granular media, ϕ_{cr} is close to zero and μ_p is close to 3 [*Mavko et al.*, 2009]. Because porosity loss in the crust depends on crustal viscosity, crustal heating and thickening during episodes of magmatism may accelerate compaction, thereby influencing permeability [*Kiefer*, 2013]. Changes in porosity ϕ from viscous flow can be modeled as

$$\frac{d\phi}{dt} = -\phi\frac{P}{\mu_{\text{crust}}} \tag{A11}$$

where μ_{crust} is the crustal viscosity and P is the lithostatic pressure [*Fowler*, 1985].

We adopt the viscosity of Maryland diabase [*Turcotte and Schubert*, 2014] for the rheology of the Martian crust:

$$\mu_{\text{crust}} = \frac{10^6}{C}{\sigma_D}^{1-n} \exp\left(\frac{E_a}{R_{\text{gas}}T}\right) \tag{A12}$$

where $C = 520\ \mathrm{MPa}^{-3}\,\mathrm{s}^{-1}$, σ_D is the deviatoric stress (assumed to be ~50 MPa, although Martian deviatoric stresses have been estimated at up to ~100 MPa [*Arkani-Hamed and Riendler*, 2002]), $n = 3$ is the stress exponent, $E_a = 356$ kJ/mol is the activation energy, and R_{gas} is the gas constant.

The porosity with increasing depth in the Martian crust is poorly constrained. We assume an initial porosity-depth profile that is consistent with the permeability profile expected for continental crust on Earth [*Manning and Ingebritsen*, 1999], scaled by the ratio of gravitational acceleration on Mars relative to Earth:

$$\log_{10}(k) = -14 - 3.2\log_{10}\left(\frac{z}{1000}\frac{g_{\mathrm{Mars}}}{g_{\mathrm{Earth}}}\right) \tag{A13}$$

and we cease compaction when the permeability drops below $10^{-20}\ \mathrm{m}^2$, which is an approximate lower limit for the permeability commonly found in terrestrial metamorphic systems [*Manning and Ingebritsen*, 1999].

When averaged over sufficient time and space, rocks (even in metamorphic systems) behave as porous media, and thus, Darcy's law can be used to relate fluid flow q to the pressure head driving the flow [*Manning and Ingebritsen*, 1999]. In one dimension, Darcy's law reduces to [e.g., *Manning and Ingebritsen*, 1999; *Saar and Manga*, 2004; *Mavko et al*., 2009]

$$q = \frac{k}{\mu_{\mathrm{fluid}}}\frac{\partial P_h}{\partial z} \tag{A14}$$

where P_h is the pressure head.

We solve equation (A11) numerically to obtain the crustal porosity, and we use equation (A10) to calculate the corresponding permeability. We then use equation (A14) to obtain the mass flux of magmatic volatiles through the crust (because of the form of equation (A14), a diffusive profile develops from the magma, through the overlying rocks, and up to the surface). If the country rock is porous, the flux of volatiles out of the magmatic system limits the buildup of buoyancy overpressure.

A7. Critical Volatile Contents

As discussed previously, we assume that buoyancy overpressure must exceed 10 MPa to trigger an eruption [*Rubin*, 1995]:

$$\left(\rho_{\mathrm{surrounding}} - \rho_{\mathrm{magma}}\right) g\, h > 10^7\ \mathrm{Pa} \tag{A15}$$

If we neglect permeable fluid escape (see section 5.3) and assume that $\rho_{\mathrm{surrounding}} = 3000\ \mathrm{kg/m}^3$ and that all bubbles rise to the top of the magma body, it is then possible to directly compute the minimum initial volatile contents required to cause at least one eruption (as a function of chamber depth and thickness). For our assumed composition (Table 2), the temperature at which the magma reaches a critical crystallinity for locking is ≤850°C. The critical volatile contents to achieve 10 MPa overpressure are then

$$X_{\mathrm{volatiles}}[\mathrm{wt\ \%}] \geq \frac{100 \times \left(10^7\ \mathrm{Pa}\right)}{\left(\frac{11{,}130\ \mathrm{kg\ m^2\ s^{-2}}}{\rho_{\mathrm{gas}}} - 3.71\ \mathrm{ms}^{-2}\right)\rho_{\mathrm{melt}} h} \tag{A16}$$

where $\rho_{\mathrm{gas}}[\mathrm{kg/m}^3] = -8548 + 127{,}811\ P^{-1.135} + 6948\ P^{0.033}$ [after *Huber et al*., 2011] with P in bars. We use equation (A16) to compute the curves in Figures 5a and 5b. Because some volatiles will escape and not all bubbles will rise, this relation gives a lower limit on the critical initial volatile contents for buoyancy-driven eruption. However, a comparison between the curves calculated with equation (A16) and the results of the full simulations (Figure 5b) shows strong agreement overall.

Acknowledgments
The authors thank the Open Earth Systems project funded by National Science Foundation grant EAR-1135382. Data sources for Mars *I/E* ratios are noted in Table 1 and cited in the text. Earth *I/E* ratios in Figure 5 are from *White et al*. [2006], as cited in the text. The modeling results are provided in the figures produced by solving the equations in the paper. Leif Karlstrom, Mark Richards, Steve Sparks, Kelly Russell, Walter Kiefer, and two anonymous reviewers provided valuable feedback on earlier versions of this work.

References

Acuna, M. H., et al. (1999), Global distribution of crustal magnetization discovered by the mars global surveyor MAG/ER experiment, *Science*, *284*(5415), 790–793.

Allard, P. (1997), Endogenous magma degassing and storage at Mount Etna, *Geophys. Res. Lett.*, *24*(17), 2219–2222, doi:10.1029/97GL02101.

Annen, C., and R. S. J. Sparks (2002), Effects of repetitive emplacement of basaltic intrusions on thermal evolution and melt generation in the crust, *Earth Planet. Sci. Lett.*, *203*(3), 937–955.

Arkani-Hamed, J., and L. Riendler (2002), Stress differences in the Martian lithosphere: Constraints on the thermal state of Mars, *J. Geophys. Res.*, *107*(E12), 5119, doi:10.1029/2002JE001851.

Bachmann, O., C. Miller, and S. De Silva (2007), The volcanic–plutonic connection as a stage for understanding crustal magmatism, *J. Volcanol. Geotherm. Res.*, *167*(1), 1–23.

Baratoux, D., M. J. Toplis, M. Monnereau, and O. Gasnault (2011), Thermal history of Mars inferred from orbital geochemistry of volcanic provinces, *Nature*, *472*(7343), 338–341.
Baratoux, D., M. Toplis, M. Monnereau, and V. Sautter (2013), The petrological expression of early Mars volcanism, *J. Geophys. Res. Planets*, *118*, 59–64.
Belien, I. B., K. V. Cashman, and A. W. Rempel (2010), Gas accumulation in particle-rich suspensions and implications for bubble populations in crystal-rich magma, *Earth Planet. Sci. Lett.*, *297*(1), 133–140.
Bird, P. (2003), An updated digital model of plate boundaries, *Geochem. Geophys. Geosyst.*, *4*(3), 1027, doi:10.1029/2001GC000252.
Blake, S. (1984), Volatile oversaturation during the evolution of silicic magma chambers as an eruption trigger, *J. Geophys. Res.*, *89*(B10), 8237–8244, doi:10.1029/JB089iB10p08237.
Bleacher, J. E., L. S. Glaze, R. Greeley, E. Hauber, S. M. Baloga, S. E. Sakimoto, D. A. Williams, and T. D. Glotch (2009), Spatial and alignment analyses for a field of small volcanic vents south of Pavonis Mons and implications for the Tharsis province, Mars, *J. Volcanol. Geotherm. Res.*, *185*(1), 96–102.
Brain, D. A., and B. M. Jakosky (1998), Atmospheric loss since the onset of the Martian geologic record: Combined role of impact erosion and sputtering, *J. Geophys. Res.*, *103*(E10), 22,689–22,694, doi:10.1029/98JE02074.
Bridges, J. C., and P. Warren (2006), The SNC meteorites: Basaltic igneous processes on Mars, *J. Geol. Soc.*, *163*(2), 229–251.
Brown, L. D., W. Zhao, K. D. Nelson, M. Hauck, D. Alsdorf, A. Ross, M. Cogan, M. Clark, X. Liu, and J. Che (1996), Bright spots, structure, and magmatism in southern Tibet from INDEPTH seismic reflection profiling, *Science*, *274*(5293), 1688–1690.
Buck, W. R., P. Einarsson, and B. Brandsdóttir (2006), Tectonic stress and magma chamber size as controls on dike propagation: Constraints from the 1975–1984 Krafla rifting episode, *J. Geophys. Res.*, *111*, B12404, doi:10.1029/2005JB003879.
Burton, M., H. Mader, and M. Polacci (2007), The role of gas percolation in quiescent degassing of persistently active basaltic volcanoes, *Earth Planet. Sci. Lett.*, *264*(1), 46–60.
Caricchi, L., C. Annen, J. Blundy, G. Simpson, and V. Pinel (2014), Frequency and magnitude of volcanic eruptions controlled by magma injection and buoyancy, *Nat. Geosci.*, *7*(2), 126–130.
Carr, M. H., R. Greeley, K. R. Blasius, J. E. Guest, and J. B. Murray (1977), Some Martian volcanic features as viewed from the Viking orbiters, *J. Geophys. Res.*, *82*(28), 3985–4015, doi:10.1029/JS082i028p03985.
Cashman, K. V., and G. Giordano (2014), Calderas and magma reservoirs, *J. Volcanol. Geotherm. Res.*, *288*, 28–45.
Chadwick, J., P. McGovern, M. Simpson, and A. Reeves (2015), Late Amazonian subsidence and magmatism of Olympus Mons, Mars, *J. Geophys. Res. Planets*, *120*, 1585–1595.
Christensen, P., H. McSween, J. Bandfield, S. Ruff, A. Rogers, V. Hamilton, N. Gorelick, M. Wyatt, B. Jakosky, and H. Kieffer (2005), Evidence for magmatic evolution and diversity on Mars from infrared observations, *Nature*, *436*(7050), 504–509.
Christopher, T., J. Blundy, K. Cashman, P. Cole, M. Edmonds, P. Smith, R. Sparks, and A. Stinton (2015), Crustal-scale degassing due to magma system destabilization and magma-gas decoupling at Soufrière Hills Volcano, Montserrat, *Geochem. Geophys. Geosyst.*, *16*, 2797–2811, doi:10.1002/2015GC005791.
Clifford, S. M. (1993), A model for the hydrologic and climatic behavior of water on Mars, *J. Geophys. Res.*, *98*(E6), 10,973–11,016, doi:10.1029/93JE00225.
Clifford, S. M., and T. J. Parker (2001), The evolution of the Martian hydrosphere: Implications for the fate of a primordial ocean and the current state of the northern plains, *Icarus*, *154*(1), 40–79.
Coffin, M. F., and O. Eldholm (1994), Large igneous provinces: Crustal structure, dimensions, and external consequences, *Rev. Geophys.*, *32*(1), 1–36, doi:10.1029/93RG02508.
Collinet, M., E. Médard, B. Charlier, J. Vander Auwera, and T. L. Grove (2015), Melting of the primitive Martian mantle at 0.5–2.2 GPa and the origin of basalts and alkaline rocks on Mars, *Earth Planet. Sci. Lett.*, *427*, 83–94.
Couch, S., R. Sparks, and M. Carroll (2003), The kinetics of degassing-induced crystallization at Soufriere Hills Volcano, Montserrat, *J. Petrol.*, *44*(8), 1477–1502.
Cox, K. (1980), A model for flood basalt volcanism, *J. Petrol.*, *21*(4), 629–650.
Crisp, J. A. (1984), Rates of magma emplacement and volcanic output, *J. Volcanol. Geotherm. Res.*, *20*(3), 177–211.
Crumpler, L., J. W. Head, and J. C. Aubele (1996), Calderas on Mars: Characteristics, structure, and associated flank deformation, *Geol. Soc. London, Spec. Publ.*, *110*(1), 307–348.
Currenti, G., and C. A. Williams (2014), Numerical modeling of deformation and stress fields around a magma chamber: Constraints on failure conditions and rheology, *Phys. Earth Planet. Inter.*, *226*, 14–27.
Daniels, K. A., and T. Menand (2015), An experimental investigation of dyke injection under regional extensional stress, *J. Geophys. Res. Solid Earth*, *120*, 2014–2035.
Degruyter, W., and C. Huber (2014), A model for eruption frequency of upper crustal silicic magma chambers, *Earth Planet. Sci. Lett.*, *403*, 117–130.
Delaney, P. T., D. D. Pollard, J. I. Ziony, and E. H. McKee (1986), Field relations between dikes and joints: Emplacement processes and paleostress analysis, *J. Geophys. Res.*, *91*(B5), 4920–4938, doi:10.1029/JB091iB05p04920.
de Silva, S. L., and P. M. Gregg (2014), Thermomechanical feedbacks in magmatic systems: Implications for growth, longevity, and evolution of large caldera-forming magma reservoirs and their super eruptions, *J. Volcanol. Geotherm. Res.*, *282*, 77–91.
Dixon, J. E., and E. M. Stolper (1995), An experimental study of water and carbon dioxide solubilities in mid-ocean ridge basaltic liquids. Part II: Applications to degassing, *J. Petrol.*, *36*(6), 1633–1646.
Dixon, J. E., D. A. Clague, and E. M. Stolper (1991), Degassing history of water, sulfur, and carbon in submarine lavas from Kilauea Volcano, Hawaii, *J. Geol.*, 371–394.
Dragoni, M., and C. Magnanensi (1989), Displacement and stress produced by a pressurized, spherical magma chamber, surrounded by a viscoelastic shell, *Phys. Earth Planet. Inter.*, *56*(3), 316–328.
Dreibus, G., and H. Wanke (1985), Mars, a volatile-rich planet, *Meteoritics*, *20*, 367–381.
Dunlop, D. J., and Ö. Özdemir (2001), *Rock Magnetism: Fundamentals and Frontiers*, vol. 3, Cambridge Univ. Press, Cambridge, U. K.
Elkins-Tanton, L. T., P. C. Hess, and E. Parmentier (2005), Possible formation of ancient crust on Mars through magma ocean processes, *J. Geophys. Res.*, *110*, E12S01, doi:10.1029/2005JE002480.
Farnetani, C. G., M. A. Richards, and M. S. Ghiorso (1996), Petrological models of magma evolution and deep crustal structure beneath hotspots and flood basalt provinces, *Earth Planet. Sci. Lett.*, *143*(1), 81–94.
Filiberto, J., J. Gross, J. Trela, and E. C. Ferré (2014), Gabbroic Shergottite Northwest Africa 6963: An intrusive sample of Mars, *Am. Mineral.*, *99*(4), 601–606.
Fowler, A. (1985), A mathematical model of magma transport in the asthenosphere, *Geophys. Astrophys. Fluid Dyn.*, *33*(1–4), 63–96.

Gaillard, F., and B. Scaillet (2009), The sulfur content of volcanic gases on Mars, *Earth Planet. Sci. Lett.*, *279*(1), 34–43.
Ghiorso, M. S., and R. O. Sack (1995), Chemical mass transfer in magmatic processes IV. A revised and internally consistent thermodynamic model for the interpolation and extrapolation of liquid-solid equilibria in magmatic systems at elevated temperatures and pressures, *Contrib. Mineral. Petrol.*, *119*(2-3), 197–212.
Greeley, R., and B. D. Schneid (1991), Magma generation on Mars: Amounts, rates, and comparisons with Earth, Moon, and Venus, *Science*, *254*(5034), 996–998, doi:10.1126/science.254.5034.996.
Grosfils, E. B. (2007), Magma reservoir failure on the terrestrial planets: Assessing the importance of gravitational loading in simple elastic models, *J. Volcanol. Geotherm. Res.*, *166*(2), 47–75.
Grott, M., and D. Breuer (2008), The evolution of the Martian elastic lithosphere and implications for crustal and mantle rheology, *Icarus*, *193*(2), 503–515.
Grott, M., A. Morschhauser, D. Breuer, and E. Hauber (2011), Volcanic outgassing of CO_2 and H_2O on Mars, *Earth Planet. Sci. Lett.*, *308*(3), 391–400.
Gruen, G., C. A. Heinrich, and K. Schroeder (2010), The Bingham Canyon porphyry Cu-Mo-Au deposit. II. Vein geometry and ore shell formation by pressure-driven rock extension, *Econ. Geol.*, *105*(1), 69–90.
Gualda, G. A., M. S. Ghiorso, R. V. Lemons, and T. L. Carley (2012), Rhyolite-MELTS: A modified calibration of MELTS optimized for silica-rich, fluid-bearing magmatic systems, *J. Petrol.*, *53*(5), 875–890.
Halbach, H., and N. D. Chatterjee (1982), An empirical Redlich-Kwong-type equation of state for water to 1,000 C and 200 kbar, *Contrib. Mineral. Petrol.*, *79*, 337–345.
Halevy, I., and J. W. Head III (2014), Episodic warming of early Mars by punctuated volcanism, *Nat. Geosci.*, *7*, 865–868, doi:10.1038/ngeo2293.
Hartmann, W. K., and G. Neukum (2001), Cratering chronology and the evolution of Mars, in *Chronology and Evolution of Mars*, Proceedings of an ISSI Workshop, Bern, Switzerland, 10–14 April 2000, edited by R. Kallenbach, J. Geiss, and W. K. Hartmann, pp. 165–194, Springer, Netherlands.
Head, J. W., M. A. Kreslavsky, and S. Pratt (2002), Northern lowlands of Mars: Evidence for widespread volcanic flooding and tectonic deformation in the Hesperian period, *J. Geophys. Res.*, *107*(E1), 5003, doi:10.1029/2000JE001445.
Hiesinger, H., and J. Head (2004), The Syrtis Major volcanic province, Mars: Synthesis from Mars global surveyor data, *J. Geophys. Res.*, *109*, E01004, doi:10.1029/2003JE002143.
Hirschmann, M. M., and A. C. Withers (2008), Ventilation of CO_2 from a reduced mantle and consequences for the early Martian greenhouse, *Earth Planet. Sci. Lett.*, *270*(1), 147–155.
Huber, C., O. Bachmann, and M. Manga (2009), Homogenization processes in silicic magma chambers by stirring and mushification (latent heat buffering), *Earth Planet. Sci. Lett.*, *283*(1), 38–47.
Huber, C., O. Bachmann, and J. Dufek (2011), Thermo-mechanical reactivation of locked crystal mushes: Melting-induced internal fracturing and assimilation processes in magmas, *Earth Planet. Sci. Lett.*, *304*(3), 443–454.
Huber, C., O. Bachmann, and J. Dufek (2012), Crystal-poor versus crystal-rich ignimbrites: A competition between stirring and reactivation, *Geology*, *40*(2), 115–118.
Humayun, M., A. Nemchin, B. Zanda, R. Hewins, M. Grange, A. Kennedy, J. Lorand, C. Göpel, C. Fieni, and S. Pont (2013), Origin and age of the earliest Martian crust from meteorite NWA 7533, *Nature*, *503*(7477), 513–516.
Huppert, H., and S. Sparks (1985), Cooling and contamination of mafic and ultramafic magmas during ascent through continental crust, *Earth Planet. Sci. Lett.*, *74*(4), 371–386.
Hutchins, K. S., and B. M. Jakosky (1996), Evolution of Martian atmospheric argon: Implications for sources of volatiles, *J. Geophys. Res.*, *101*(E6), 14,933–14,949, doi:10.1029/96JE00860.
Isherwood, R. J., L. M. Jozwiak, J. C. Jansen, and J. C. Andrews-Hanna (2013), The volcanic history of Olympus Mons from paleo-topography and flexural modeling, *Earth Planet. Sci. Lett.*, *363*, 88–96.
Jackson, J., and D. McKenzie (1988), The relationship between plate motions and seismic moment tensors, and the rates of active deformation in the Mediterranean and Middle East, *Geophys. J. Int.*, *93*(1), 45–73.
Jagoutz, O., and M. Schmidt (2012), The formation and bulk composition of modern juvenile continental crust: The Kohistan arc, *Chem. Geol.*, *298*, 79–96.
Jakosky, B. M., and J. H. Jones (1997), The history of Martian volatiles, *Rev. Geophys.*, *35*(1), 1–16, doi:10.1029/96RG02903.
Jakosky, B. M., R. Lin, J. Grebowsky, J. Luhmann, D. Mitchell, G. Beutelschies, T. Priser, M. Acuna, L. Andersson, and D. Baird (2015), The Mars Atmosphere and Volatile Evolution (MAVEN) mission, *Space Sci. Rev.*, 1–46.
Jellinek, A., C. Johnson, and G. Schubert (2008), Constraints on the elastic thickness, heat flow, and melt production at early Tharsis from topography and magnetic field observations, *J. Geophys. Res.*, *113*, E09004, doi:10.1029/2007JE003005.
Jellinek, A. M., and D. J. DePaolo (2003), A model for the origin of large silicic magma chambers: Precursors of caldera-forming eruptions, *Bull. Volcanol.*, *65*(5), 363–381.
Jicha, B. R., and O. Jagoutz (2015), Magma production rates for intraoceanic arcs, *Elements*, *11*(2), 105–111.
Johnson, C. L., and R. J. Phillips (2005), Evolution of the Tharsis region of Mars: Insights from magnetic field observations, *Earth Planet. Sci. Lett.*, *230*(3), 241–254.
Johnson, S. S., M. A. Mischna, T. L. Grove, and M. T. Zuber (2008), Sulfur-induced greenhouse warming on early Mars, *J. Geophys. Res.*, 113, E08005, doi:10.1029/2007JE002962.
Karlstrom, L., and M. Manga (2009), Magma siphoning and the mechanics of Large Igneous Province eruptions, paper presented at AGU Fall Meeting Abstracts.
Karlstrom, L., and M. Richards (2011), On the evolution of large ultramafic magma chambers and timescales for flood basalt eruptions, *J. Geophys. Res.*, *116*, B08216, doi:10.1029/2010JB008159.
Karlstrom, L., J. Dufek, and M. Manga (2010), Magma chamber stability in arc and continental crust, *J. Volcanol. Geotherm. Res.*, *190*(3), 249–270.
Karlstrom, L., M. L. Rudolph, and M. Manga (2012), Caldera size modulated by the yield stress within a crystal-rich magma reservoir, *Nat. Geosci.*, *5*(6), 402–405.
Keppler, H. (1999), Experimental evidence for the source of excess sulfur in explosive volcanic eruptions, *Science*, *284*(5420), 1652–1654.
Kiefer, W. S. (2003), Melting in the Martian mantle: Shergottite formation and implications for present-day mantle convection on Mars, *Meteorit. Planet. Sci.*, *38*(12), 1815–1832.
Kiefer, W. S. (2004), Gravity evidence for an extinct magma chamber beneath Syrtis Major, Mars: A look at the magmatic plumbing system, *Earth Planet. Sci. Lett.*, *222*(2), 349–361.
Kiefer, W. S. (2013), Gravity constraints on the subsurface structure of the Marius Hills: The magmatic plumbing of the largest lunar volcanic dome complex, *J. Geophys. Res. Planets*, *118*, 733–745, doi:10.1029/2012JE004111.

Korenaga, J., P. B. Kelemen, and W. S. Holbrook (2002), Methods for resolving the origin of large igneous provinces from crustal seismology, *J. Geophys. Res.*, *107*(B9), 2178, doi:10.1029/2001JB001030.
Kress, V. C., and I. S. Carmichael (1991), The compressibility of silicate liquids containing Fe_2O_3 and the effect of composition, temperature, oxygen fugacity and pressure on their redox states, *Contrib. Mineral. Petrol.*, *108*(1-2), 82–92.
Leeman, W. P., C. Annen, and J. Dufek (2008), Snake River Plain–Yellowstone silicic volcanism: Implications for magma genesis and magma fluxes, *Geol. Soc. London, Spec. Publ.*, *304*(1), 235–259.
Li, Q., and W. S. Kiefer (2007), Mantle convection and magma production on present-day Mars: Effects of temperature-dependent rheology, *Geophys. Res. Lett.*, *34*, L16203, doi:10.1029/2007GL030544.
Lillis, R. J., H. V. Frey, and M. Manga (2008a), Rapid decrease in Martian crustal magnetization in the Noachian era: Implications for the dynamo and climate of early Mars, *Geophys. Res. Lett.*, *35*, L14203, doi:10.1029/2008GL034338.
Lillis, R. J., H. V. Frey, M. Manga, D. L. Mitchell, R. P. Lin, M. H. Acuña, and S. W. Bougher (2008b), An improved crustal magnetic field map of Mars from electron reflectometry: Highland volcano magmatic history and the end of the Martian dynamo, *Icarus*, *194*(2), 575–596.
Lillis, R. J., J. Dufek, J. E. Bleacher, and M. Manga (2009), Demagnetization of crust by magmatic intrusion near the Arsia Mons volcano: Magnetic and thermal implications for the development of the Tharsis province, Mars, *J. Volcanol. Geotherm. Res.*, *185*(1), 123–138.
Lillis, R. J., J. Dufek, W. S. Kiefer, B. A. Black, M. Manga, J. A. Richardson, and J. E. Bleacher (2015), The Syrtis Major volcano, Mars: A multidisciplinary approach to interpreting its magmatic evolution and structural development, *J. Geophys. Res. Planets*, *120*, 1476–1496, doi:10.1002/2014JE004774.
Longhi, J., and V. Pan (1989), The parent magmas of the SNC meteorites paper presented at Lunar and Planetary Science Conference Proceedings.
Lowry, A. R., and S. Zhong (2003), Surface versus internal loading of the Tharsis rise, Mars, *J. Geophys. Res.*, *108*(E9), 5099, doi:10.1029/2003JE002111.
Malfait, W. J., R. Seifert, S. Petitgirard, J. Perrillat, M. Mezouar, T. Ota, E. Nakamura, P. Lerch, and C. Sanchez-Valle (2014), Supervolcano eruptions driven by melt buoyancy in large silicic magma chambers, *Nat. Geosci.*, *7*(2), 122–125.
Manga, M., and H. Stone (1995), Low Reynolds number motion of bubbles, drops and rigid spheres through fluid–fluid interfaces, *J. Fluid Mech.*, *287*, 279–298.
Manning, C., and S. Ingebritsen (1999), Permeability of the continental crust: Implications of geothermal data and metamorphic systems, *Rev. Geophys.*, *37*(1), 127–150, doi:10.1029/1998RG900002.
Marsh, B. (1981), On the crystallinity, probability of occurrence, and rheology of lava and magma, *Contrib. Mineral. Petrol.*, *78*(1), 85–98.
Mavko, G., T. Mukerji, and J. Dvorkin (2009), *The Rock Physics Handbook: Tools for Seismic Analysis of Porous Media*, Cambridge Univ. Press, Cambridge, U. K.
McCubbin, F. M., A. Smirnov, H. Nekvasil, J. Wang, E. Hauri, and D. H. Lindsley (2010), Hydrous magmatism on Mars: A source of water for the surface and subsurface during the Amazonian, *Earth Planet. Sci. Lett.*, *292*(1), 132–138.
McEwen, A. S., M. C. Malin, M. H. Carr, and W. K. Hartmann (1999), Voluminous volcanism on early Mars revealed in Valles Marineris, *Nature*, *397*(6720), 584–586.
McGovern, P. J., S. C. Solomon, D. E. Smith, M. T. Zuber, M. Simons, M. A. Wieczorek, R. J. Phillips, G. A. Neumann, O. Aharonson, and J. W. Head (2002), Localized gravity/topography admittance and correlation spectra on Mars: Implications for regional and global evolution, *J. Geophys. Res.*, *107*(E12), 5136, doi:10.1029/2002JE001854.
McGovern, P. J., M. E. Rumpf, and J. R. Zimbelman (2013), The influence of lithospheric flexure on magma ascent at large volcanoes on Venus, *J. Geophys. Res. Planets*, *118*, 2423–2437.
McGovern, P. J., E. B. Grosfils, G. A. Galgana, J. K. Morgan, M. E. Rumpf, J. R. Smith, and J. R. Zimbelman (2015), Lithospheric flexure and volcano basal boundary conditions: Keys to the structural evolution of large volcanic edifices on the terrestrial planets, *Geol. Soc. London, Spec. Publ.*, *401*(1), 219–237.
McSween, H. Y., M. B. Wyatt, R. Gellert, J. Bell, R. V. Morris, K. E. Herkenhoff, L. S. Crumpler, K. A. Milam, K. R. Stockstill, and L. L. Tornabene (2006), Characterization and petrologic interpretation of olivine-rich basalts at Gusev Crater, Mars, *J. Geophys. Res.*, *111*, E02S10, doi:10.1029/2005JE002477.
Mège, D., and P. Masson (1996a), A plume tectonics model for the Tharsis province, Mars, *Planet. Space Sci.*, *44*(12), 1499–1546.
Mège, D., and P. Masson (1996b), Stress models for Tharsis formation, Mars, *Planet. Space Sci.*, *44*(12), 1471–1497.
Menand, T., K. Daniels, and P. Benghiat (2010), Dyke propagation and sill formation in a compressive tectonic environment, *J. Geophys. Res.*, *115*, B08201, doi:10.1029/2009JB00679.
Michaut, C., and C. Jaupart (2006), Ultra-rapid formation of large volumes of evolved magma, *Earth Planet. Sci. Lett.*, *250*(1), 38–52.
Mitchell, D., R. Lillis, R. Lin, J. Connerney, and M. Acuña (2007), A global map of Mars' crustal magnetic field based on electron reflectometry, *J. Geophys. Res.*, *112*, E01002, doi:10.1029/2005JE002564.
Mysen, B. O., D. Virgo, R. K. Popp, and C. M. Bertka (1998), The role of H_2O in Martian magmatic systems, *Am. Mineral.*, *83*, 942–946.
Neumann, G., M. Zuber, M. Wieczorek, P. McGovern, F. Lemoine, and D. Smith (2004), Crustal structure of Mars from gravity and topography, *J. Geophys. Res.*, *109*, E08002, doi:10.1029/2004JE002262.
Newman, S., and J. B. Lowenstern (2002), VolatileCalc: A silicate melt–H_2O–CO_2 solution model written in Visual Basic for Excel, *Comput. Geosci.*, *28*(5), 597–604.
Nimmo, F., and D. Stevenson (2000), Influence of early plate tectonics on the thermal evolution and magnetic field of Mars, *J. Geophys. Res.*, *105*(E5), 11,969–11,979, doi:10.1029/1999JE001216.
Ogawa, Y., and M. Manga (2007), Thermal demagnetization of Martian upper crust by magma intrusion, *Geophys. Res. Lett.*, *34*, L16302, doi:10.1029/2007GL030565.
O'Neill, C., A. Lenardic, A. Jellinek, and W. Kiefer (2007), Melt propagation and volcanism in mantle convection simulations, with applications for Martian volcanic and atmospheric evolution, *J. Geophys. Res.*, *112*, E07003, doi:10.1029/2006JE002799.
Phillips, R. J., N. H. Sleep, and W. B. Banerdt (1990), Permanent uplift in magmatic systems with application to the Tharsis region of Mars, *J. Geophys. Res.*, *95*(B4), 5089–5100, doi:10.1029/JB095iB04p05089.
Phillips, R. J., et al. (2001), Ancient geodynamics and global-scale hydrology on Mars, *Science*, *291*(5513), 2587–2591, doi:10.1126/science.1058701.
Pinel, V., and C. Jaupart (2004), Magma storage and horizontal dyke injection beneath a volcanic edifice, *Earth Planet. Sci. Lett.*, *221*(1), 245–262.
Richards, M., E. Contreras-Reyes, C. Lithgow-Bertelloni, M. Ghiorso, and L. Stixrude (2013), Petrological interpretation of deep crustal intrusive bodies beneath oceanic hotspot provinces, *Geochem. Geophys. Geosyst.*, *14*, 604–619, doi:10.1029/2012GC004448.
Ridley, V. A., and M. A. Richards (2010), Deep crustal structure beneath large igneous provinces and the petrologic evolution of flood basalts, *Geochem. Geophys. Geosyst.*, *11*, Q09006, doi:10.1029/2009GC002935.
Righter, K., H. Yang, G. Costin, and R. Downs (2008), Oxygen fugacity in the Martian mantle controlled by carbon: New constraints from the nakhlite MIL 03346, *Meteorit. Planet. Sci.*, *43*(10), 1709–1723.

Righter, K., K. Pando, and L. Danielson (2009), Experimental evidence for sulfur-rich Martian magmas: Implications for volcanism and surficial sulfur sources, *Earth Planet. Sci. Lett.*, *288*(1), 235–243.
Robbins, S. J., G. Di Achille, and B. M. Hynek (2011), The volcanic history of Mars: High-resolution crater-based studies of the calderas of 20 volcanoes, *Icarus*, *211*(2), 1179–1203.
Roberts, J. H., R. J. Lillis, and M. Manga (2009), Giant impacts on early Mars and the cessation of the Martian dynamo, *J. Geophys. Res.*, *114*, E04009, doi:10.1029/2008JE003287.
Roeder, P., and R. Emslie (1970), Olivine-liquid equilibrium, *Contrib. Mineral. Petrol.*, *29*(4), 275–289.
Rubin, A. M. (1995), Propagation of magma-filled cracks, *Annu. Rev. Earth Planet. Sci.*, *23*, 287–336.
Rudnick, R. L. (1995), Making continental crust, *Nature*, *378*(6557), 571–577.
Rudnick, R. L., and D. M. Fountain (1995), Nature and composition of the continental crust: A lower crustal perspective, *Rev. Geophys.*, *33*(3), 267–309, doi:10.1029/95RG01302.
Saar, M., and M. Manga (2004), Depth dependence of permeability in the Oregon Cascades inferred from hydrogeologic, thermal, seismic, and magmatic modeling constraints, *J. Geophys. Res.*, *109*, B04204, doi:10.1029/2003JB002855.
Sahimi, M. (1994), *Applications of Percolation Theory*, CRC Press, Boca Raton, Fla.
Schubert, G., S. C. Solomon, D. Turcotte, M. Drake, and N. Sleep (1993), Origin and thermal evolution of Mars, in *Mars*, edited by H. H. Kieffer et al., pp. 147–183, Univ. of Arizona Press, Tucson.
Scott, E. D., L. Wilson, and J. W. Head (2002), Emplacement of giant radial dikes in the northern Tharsis region of Mars, *J. Geophys. Res.*, *107*(E4), 5019, doi:10.1029/2000JE001431.
Sekhar, P., and S. D. King (2014), 3D spherical models of Martian mantle convection constrained by melting history, *Earth Planet. Sci. Lett.*, *388*, 27–37.
Shaw, H. R. (1980), The fracture mechanisms of magma transport from the mantle to the surface, *Phys. Magmat. Processes*, *64*, 201–264.
Shinohara, H. (2008), Excess degassing from volcanoes and its role on eruptive and intrusive activity, *Rev. Geophys.*, *46*, RG4005, doi:10.1029/2007RG000244.
Sleep, N. H., and R. J. Phillips (1985), Gravity and lithospheric stress on the terrestrial planets with reference to the Tharsis region of Mars, *J. Geophys. Res.*, *90*(B6), 4469–4489, doi:10.1029/JB090iB06p04469.
Solomon, S. C., and J. W. Head (1982), Evolution of the Tharsis province of Mars: The importance of heterogeneous lithospheric thickness and volcanic construction, *J. Geophys. Res.*, *87*(B12), 9755–9774, doi:10.1029/JB087iB12p09755.
Šrámek, O., and S. Zhong (2012), Martian crustal dichotomy and Tharsis formation by partial melting coupled to early plume migration, *J. Geophys. Res.*, *117*, E01005, doi:10.1029/2011JE003867.
Stanley, B. D., M. M. Hirschmann, and A. C. Withers (2011), CO_2 solubility in Martian basalts and Martian atmospheric evolution, *Geochim. Cosmochim. Acta*, *75*(20), 5987–6003.
Tait, S., C. Jaupart, and S. Vergniolle (1989), Pressure, gas content and eruption periodicity of a shallow, crystallising magma chamber, *Earth Planet. Sci. Lett.*, *92*(1), 107–123.
Tajika, E., and S. Sasaki (1996), Magma generation on Mars constrained from an ^{40}Ar degassing model, *J. Geophys. Res.*, *101*(E3), 7543–7554, doi:10.1029/95JE03863.
Tanaka, K. L., M. P. Golombek, and W. B. Banerdt (1991), Reconciliation of stress and structural histories of the Tharsis region of Mars, *J. Geophys. Res.*, *96*(E1), 15,617–15,633, doi:10.1029/91JE01194.
Tanaka, K. L., J. A. Skinner, and T. M. Hare (2005), Geologic map of the northern plains of Mars, U.S. Geol. Surv. Misc. Invest. Ser. Map I-2888.
Tikoff, B., and C. Teyssier (1994), Strain modeling of displacement-field partitioning in transpressional orogens, *J. Struct. Geol.*, *16*(11), 1575–1588.
Turcotte, D. L., and G. Schubert (2014), *Geodynamics*, Cambridge Univ. Press, Cambridge, U. K.
Usui, T., H. Y. McSween, and C. Floss (2008), Petrogenesis of olivine-phyric shergottite Yamato 980459, revisited, *Geochim. Cosmochim. Acta*, *72*(6), 1711–1730.
Usui, T., C. M. Alexander, J. Wang, J. I. Simon, and J. H. Jones (2012), Origin of water and mantle–crust interactions on Mars inferred from hydrogen isotopes and volatile element abundances of olivine-hosted melt inclusions of primitive shergottites, *Earth Planet. Sci. Lett.*, *357*, 119–129.
Wadhwa, M. (2001), Redox state of Mars' upper mantle and crust from Eu anomalies in shergottite pyroxenes, *Science*, *291*(5508), 1527–1530, doi:10.1126/science.291.5508.1527.
Ward, K. M., G. Zandt, S. L. Beck, D. H. Christensen, and H. McFarlin (2014), Seismic imaging of the magmatic underpinnings beneath the Altiplano-Puna volcanic complex from the joint inversion of surface wave dispersion and receiver functions, *Earth Planet. Sci. Lett.*, *404*, 43–53.
Watters, T. R. (1993), Compressional tectonism on Mars, *J. Geophys. Res.*, *98*(E9), 17,049–17,060, doi:10.1029/93JE01138.
Weis, P., T. Driesner, and C. A. Heinrich (2012), Porphyry-copper ore shells form at stable pressure-temperature fronts within dynamic fluid plumes, *Science*, *338*(6114), 1613–1616, doi:10.1126/science.1225009.
Wetzel, D. T., M. J. Rutherford, S. D. Jacobsen, E. H. Hauri, and A. E. Saal (2013), Degassing of reduced carbon from planetary basalts, *Proc. Natl. Acad. Sci. U.S.A.*, *110*(20), 8010–8013, doi:10.1073/pnas.1219266110.
White, S. M., J. A. Crisp, and F. J. Spera (2006), Long-term volumetric eruption rates and magma budgets, *Geochem. Geophys. Geosyst.*, *7*, Q03010, doi:10.1029/2005GC001002.
Willemann, R. J., and D. L. Turcotte (1982), The role of lithospheric stress in the support of the Tharsis rise, *J. Geophys. Res.*, *87*(B12), 9793–9801, doi:10.1029/JB087iB12p09793.
Wilson, L., and J. W. Head (1994), Mars: Review and analysis of volcanic eruption theory and relationships to observed landforms, *Rev. Geophys.*, *32*(3), 221–263, doi:10.1029/94RG01113.
Wilson, L., and J. W. Head (2002), Tharsis-radial graben systems as the surface manifestation of plume-related dike intrusion complexes: Models and implications, *J. Geophys. Res.*, *107*(E8), 5057, doi:10.1029/2001JE001593.
Wilson, L., E. D. Scott, and J. W. Head (2001), Evidence for episodicity in the magma supply to the large Tharsis volcanoes, *J. Geophys. Res.*, *106*(E1), 1423–1433, doi:10.1029/2000JE001280.
Wray, J. J., S. T. Hansen, J. Dufek, G. A. Swayze, S. L. Murchie, F. P. Seelos, J. R. Skok, R. P. Irwin III, and M. S. Ghiorso (2013), Prolonged magmatic activity on Mars inferred from the detection of felsic rocks, *Nat. Geosci.*, *6*(12), 1013–1017.
Zhang, X., and R. H. Davis (1991), The rate of collisions due to Brownian or gravitational motion of small drops, *J. Fluid Mech.*, *230*, 479–504.
Zoback, M. L. (1992), First-and second-order patterns of stress in the lithosphere: The world stress map project, *J. Geophys. Res.*, *97*, 11,703–11,728, doi:10.1029/92JB00132.
Zuber, M. T. (2001), The crust and mantle of Mars, *Nature*, *412*(6843), 220–227.